A DYNAMIC REPRESENTATION OF A SALIENT POLE SYNCHRONOUS GENERATOR

Robert Alan Duin

and

Donald Bruce Russell

Library
U. S. Naval Postgraduate School
Monterey, California

1-48

GEN	GENERATORS
ALT	ALTERNATING CURRENT
ANB	ANALOG COMPUTERS

A DYNAMIC REPRESENTATION OF A SALIENT POLE SYNCHRONOUS GENERATOR

by

ROBERT ALAN DUIN, LIEUTENANT, U.S. COAST GUARD
B.S., U.S. Coast Guard Academy, 1948

and

DONALD BRUCE RUSSELL, LIEUTENANT, U.S. COAST GUARD
B.S., U.S. Coast Guard Academy, 1949

SUBMITTED IN PARTIAL FULFILLMENT OF THE
REQUIREMENTS FOR THE DEGREE OF
NAVAL ENGINEER
at the
MASSACHUSETTS INSTITUTE OF TECHNOLOGY
June 1955

A DYNAMIC REPRESENTATION OF A SALIENT POLE SYNCHRONOUS GENERATOR

by

ROBERT A. DUIN
Lieutenant, U. S. Coast Guard

and

DONALD B. RUSSELL
Lieutenant, U. S. Coast Guard

Postgraduate School
Monterey, California

Submitted to the Department of Naval Architecture and Marine Engineering on May 23, 1955, in partial fulfillment of the requirements for the degree of Naval Engineer.

ABSTRACT

This thesis develops a block diagram representation of a salient pole synchronous generator. This representation in its final form provides an accurate means for analyzing the machine by analog computer methods.

Linear volt-ampere equations describing the synchronous alternator are developed from the basic equations for the various machine circuits by means of matrix algebra. Using these linear volt-ampere equations and making certain simplifying assumptions, a single time constant computer block diagram which represents the alternator and its connected load is developed. The nonlinear effects of saturation are introduced at a single point in this block diagram.

The validity of the representation is shown by a comparison of steady state and transient phenomena as obtained experimentally from the alternator and analytically from the computer representation of the alternator. The steady state results show exact agreement of the open circuit condition and only slight divergence in the upper regions of saturation for the experimental and computer curves describing operation at both zero and unity power factors with rated armature current.

Transient phenomena are measured by application of both load steps and field excitation steps for three widely separated conditions of loading. Agreement between experimental and computer transients is excellent for the load changes and acceptable for the field excitation changes.

28933

Conclusions

(1) The block diagram developed is a valid representation of the synchronous alternator.

(2) The final representation is in a form readily adaptible to computer presentation.

(3) The experimental and computer steady state characteristics curves diverge somewhat at high values of field excitation for both unity and zero power factor loads. This divergence will decrease for intermediate values of loading.

Recommendations

The recommendation is made that the following points should be investigated further:

(1) Methods to reduce the steady state errors at high values of field excitation with both zero and unity power factor loads.

(2) Plausibility of including the effects of armature transients and amortisseur subtransients in the alternator block diagram.

(3) A method to properly account for speed variations in the representation.

(4) Study of inclusion of unbalanced loads in the generator-load representation.

ACKNOWLEDGEMENTS

The authors are indebted to Professor D. C. White of the Electrical Engineering Department, Massachusetts Institute of Technology, for his advice and guidance; to Mr. V. Haas, Mr. M. Riaz, and Mr. M. A. Xavier of the Energy Conversion Group, Massachusetts Institute of Technology, for their great interest and assistance in the development of this thesis; to Miss Leonora Coronella for her patience, forbearance, and skill in preparing the thesis in its final form; and to the large number of people at the Massachusetts Institute of Technology who helped make this project an enjoyable and educative experience.

TABLE OF CONTENTS

	Page
ABSTRACT	ii
ACKNOWLEDGEMENTS	iv
I. INTRODUCTION	1
II. PROCEDURE	3
III. RESULTS	7
IV. DISCUSSION OF RESULTS	15
V. CONCLUSIONS	21
VI. RECOMMENDATIONS	22
VII. APPENDIX	23
A. Development of the Linear Volt-Ampere Equations Describing the Synchronous Alternator	24
B. Development of a Computer Block Diagram Representation of the Synchronous Alternator	36
C. Experimental Determination of Machine Parameters and Transient Phenomena	46
D. Computer Determination of Transient Phenomena	57
E. Summary of Data and Calculations	70
F. Equipment	72
G. Literature Citations	73

I

INTRODUCTION

The transient performance of synchronous machines has been the subject of many careful investigations which have resulted in a considerable amount of data representing operation under all types of conditions. Most of these investigations have been based upon linear theory in order to keep the analysis as clear and uncomplicated as possible. When included in these analyses, nonlinear effects were introduced by adjustment of machine parameters at a particular condition of operation and were valid only at that condition.

A more recent investigation (11)(12) by the Energy Conversion Group, Massachusetts Institute of Technology, adopted a somewhat different approach. This investigation was primarily concerned with the voltage regulatory problem of an alternating current generator system. Since the various dynamic problems associated with regulation, such as load changes, faults, and switching, as well as the many components of the system itself, are nonlinear, a completely linear analysis was impossible. Consequently, one of the purposes of this investigation was the development of a block diagram representation of the voltage regulatory system, including nonlinear effects, which would be suitable for a study of the problem using an analogue computer.

In the portion of the study concerned with the synchronous alternator the Energy Conversion Group was successful in obtaining a computer representation of the alternator which proved to be valid with a zero power factor load.

The purpose of this report is to present the steps which were followed in the development of a dynamic computer block diagram representation of a synchronous alternator, including nonlinear characteristics, which is valid for any type of transient disturbance and for loads of power factors from zero to one inclusive.

II

PROCEDURE

The procedure followed in developing the computer block diagram representation of a synchronous alternator and testing its validity can be divided into the following steps:

Development of the Linear Volt-Ampere Equations Describing the Synchronous Alternator

In this portion of the report the electrical equations of motion for the stator and rotor were written and, by a series of transformations, were changed to direct and quadrature two-axis components (10). The equations for the synchronous machine were first developed in motor form and were then changed to the generator form. Throughout this development matrix algebra was used to provide a compactness of form with the transformations following a path from three-phase components to Lyon's symmetrical components, to forward and backward rotating components, and finally to Park's direct and quadrature two-axis components. In order to obtain a final set of volt-ampere relationships which are linear differential equations with constant coefficients, it was necessary to assume constant speed operation.

Appendix A is a more thorough description of this portion of the report.

Development of a Computer Block Diagram Representation of the Synchronous Alternator and its Connected Load

A block diagram was developed from the volt-ampere equations

describing the synchronous alternator. In order to include a load representation in this block diagram a vector diagram describing the machine in two-axis components was constructed. Since the block diagram developed was not suitable for direct application to an analog computer, it was necessary to change this block diagram to computer form and include a valid representation of the nonlinear characteristics of the synchronous alternator.

Appendix B describes the development of a computer representation more completely.

Experimental Determination of Machine Parameters and Transients Phenomena

After choosing a suitable synchronous generator, the machine parameters were determined from the following tests and measurements: slip test, open circuit test, short circuit test, and a measurement of the field time constant. This experimental work provided the necessary machine parameters which were then converted to per unit values in the reciprocal system described by reference 8. Resulting from this conversion were the per unit values necessary to complete the computer block diagram representation. These are listed below.

R_f = per unit field resistance including field rheostat and external circuit resistances,

X_{md} = per unit magnetizing reactance,

X_{fl} = per unit field leakage reactance,

X_{al} = per unit armature leakage reactance,

and the nonlinear relation between resultant open circuit field current, $i_{f_{oc}}$, and "air gap" field current, $i_{f_{ag}}$.

The transient characteristics of the synchronous generator were determined at three widely separated load conditions: pure inductive load (pF = 0), pure resistive load (pF = 1), and a combination inductive-resistive load (pF = 0.752). The choice of load also determined the remaining two blocks, $\sqrt{K_2(\theta)^2 + 1}$ and $K_1(\theta)$, in the load portion of the computer representation. For each of these load conditions the dynamic effects upon armature terminal voltage, armature current, and field voltage were determined by oscillograms when making the following setp changes: no load to full load, full load to no load, and a field voltage step.

The final computer block diagram representation was based upon the assumption that the machine speed remained constant. During the determination of the transient phenomena, the machine speed varied upon application of the various step changes, the amount of variation depending upon the load condition. An oscillogram was taken of this speed transient in order to determine the effect of the speed variation upon the other transients measured.

Appendix C is a more complete description of the experimental determination of machine parameters and transient phenomena.

Computer Determination of Transient Phenomena

The alternator representation obtained should be suitable for analytic study and solution by analog computer methods, and was developed with this object in mind. In order to test the validity of the alternator representation, the solution of the block diagram should be checked with transient and steady-state values obtained by direct experimentation on the test machine. An initial computer test was,

therefore, to obtain characteristic curves of steady-state relationships between field excitation and generator voltage under various conditions of loading. These curves should compare with the saturation curves experimentally obtained. The computer study of transient phenomena was made duplicating the field excitation and load conditions which were used in the experimental transient study.

Appendix D describes the computer analysis more completely.

III

RESULTS

Figure I presents the block diagram representation of the salient pole synchronous generator. This representation was used to determine various steady state and transient terminal voltage responses from an analog computer study. An experimental study was also made duplicating the conditions used for obtaining the computer responses. This section of the thesis correlates the results of the experimental and computer work and proves the validity of the developed block diagram.

Figure XI presents a comparison of the saturation curves obtained by both experimental and computer study at no-load and at zero and unity-power factors with rated armature current.

Figures II through X present a comparison of the transient responses of the terminal voltage for changes in load and field excitation as obtained by both computer and experimental studies. The initial and final voltages in the case of each transient were adjusted on the experimental curves to coincide with the initial and final voltages obtained from the computer curves. This was made necessary because the computer study was carried out assuming constant speed, whereas actually the experimental transients were accompanied by generator speed changes.

The computer representation was developed by neglecting armature transients and subtransient effects due to the amortisseur

windings. The computer transients reflect this omission in the theoretical development by a sudden change at the point where the transient was initiated. These transient and subtransient reactance changes are present in the experimental curves near the point of transient initiation; however, they die out very rapidly.

Table I is a comparative tabulation of the time constants obtained from the experimental and computer transients as measured when neglecting those transients due to armature reactance and amortisseur subtransient reactance.

TABLE I

TIME CONSTANT COMPARISON

	Experimental	Computer
Power factor = 0		
Full load to no load	0.10	0.105
No load to full load	0.125	0.145
Field step	0.155	0.20
Power factor = 1.0		
Full load to no load	0.125	0.13
No load to full load	0.13	0.14
Field step	0.148	0.175
Power factor = 0.752		
Full load to no load	0.11	0.10
No load to full load	0.14	0.145
Field step	0.145	0.195

FIGURE I

BLOCK DIAGRAM REPRESENTATION FOR THE SALIENT POLE SYNCHRONOUS ALTERNATOR

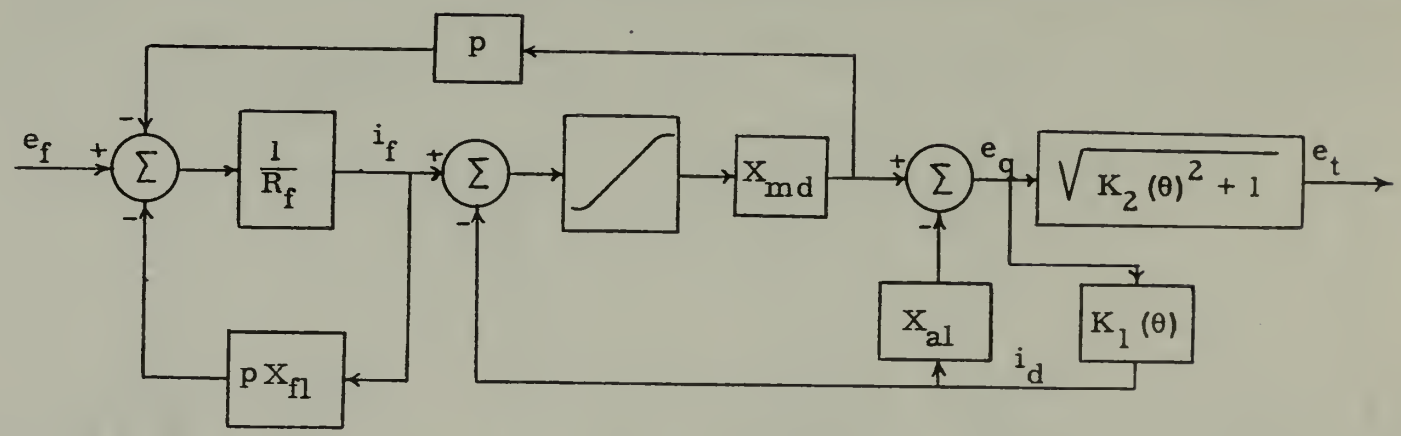

Definitions (all values in per unit)

e_f = field voltage

e_q = quadrature axis armature voltage

e_t = armature terminal voltage

i_f = field current

i_d = direct axis armature current

R_f = field resistance

X_{fl} = field leakage reactance

X_{md} = magnetizing reactance

X_{al} = armature leakage reactance

$$p = \frac{d}{d(\omega_o t)}$$

$$K_1(\theta) = \frac{X_q \cos^2 \theta}{Z_L(Z_L + X_q \sin \theta)} + \frac{\sin \theta}{Z_L}$$

$$K_2(\theta) = \frac{X_q \cos \theta}{Z_L + X_q \sin \theta}$$

X_q = quadrature axis synchronous reactance

Z_L = load impedance

θ = phase angle

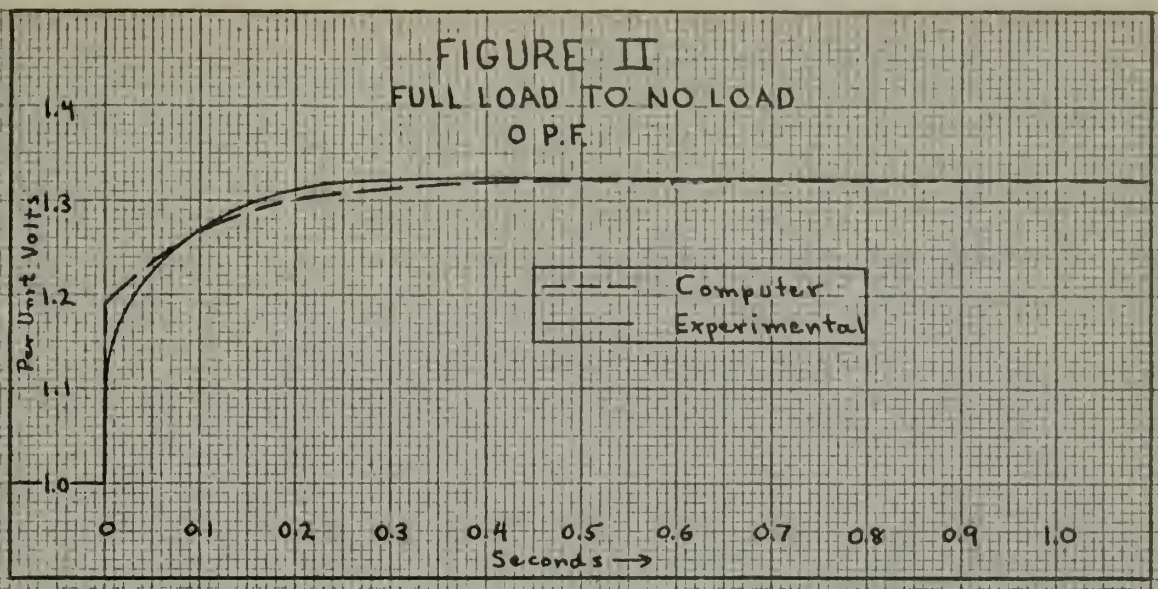

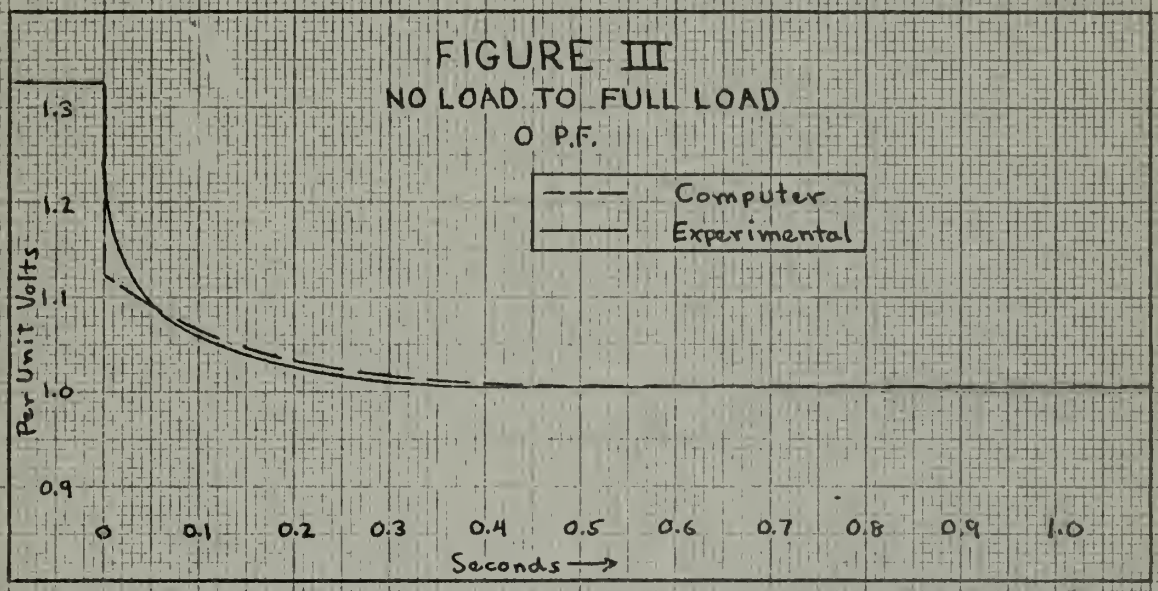

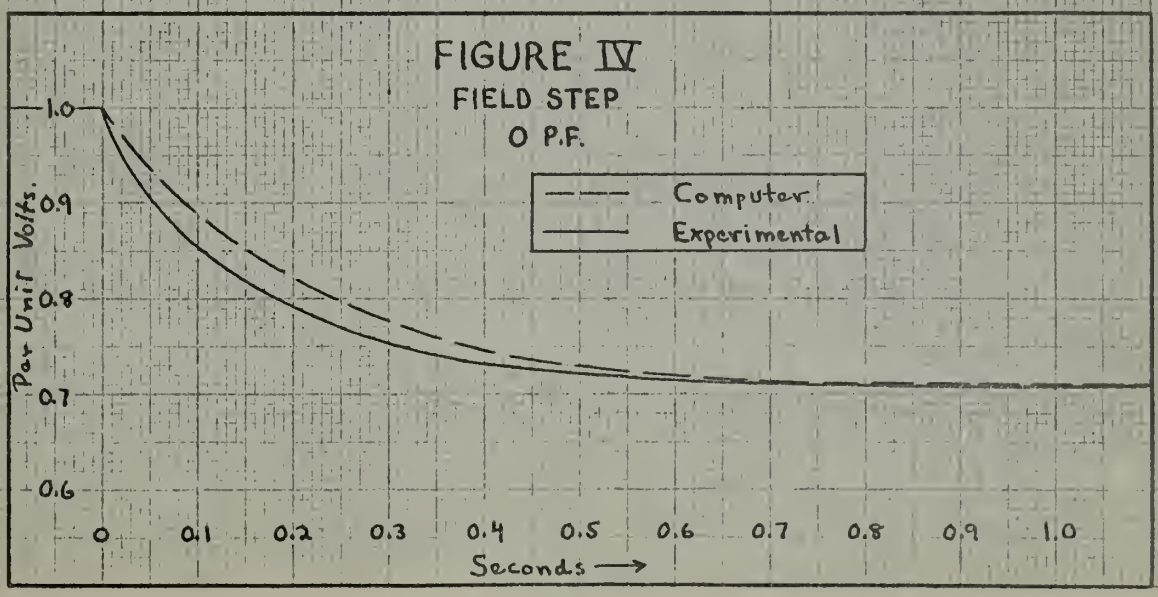

RAD - DBR
MAY '55

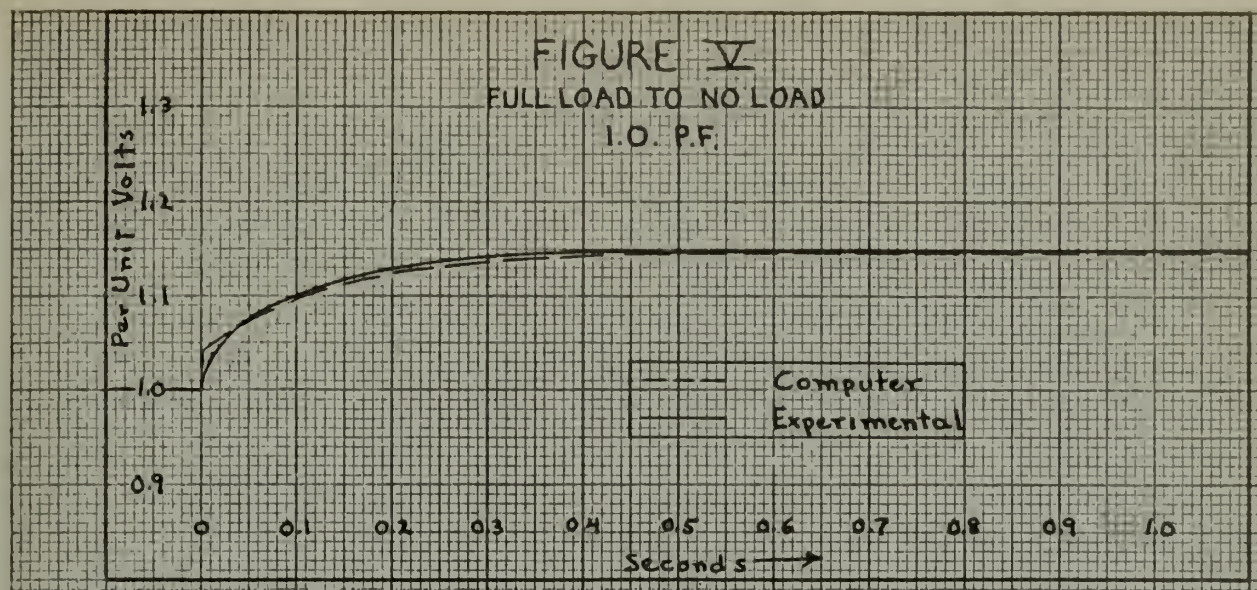

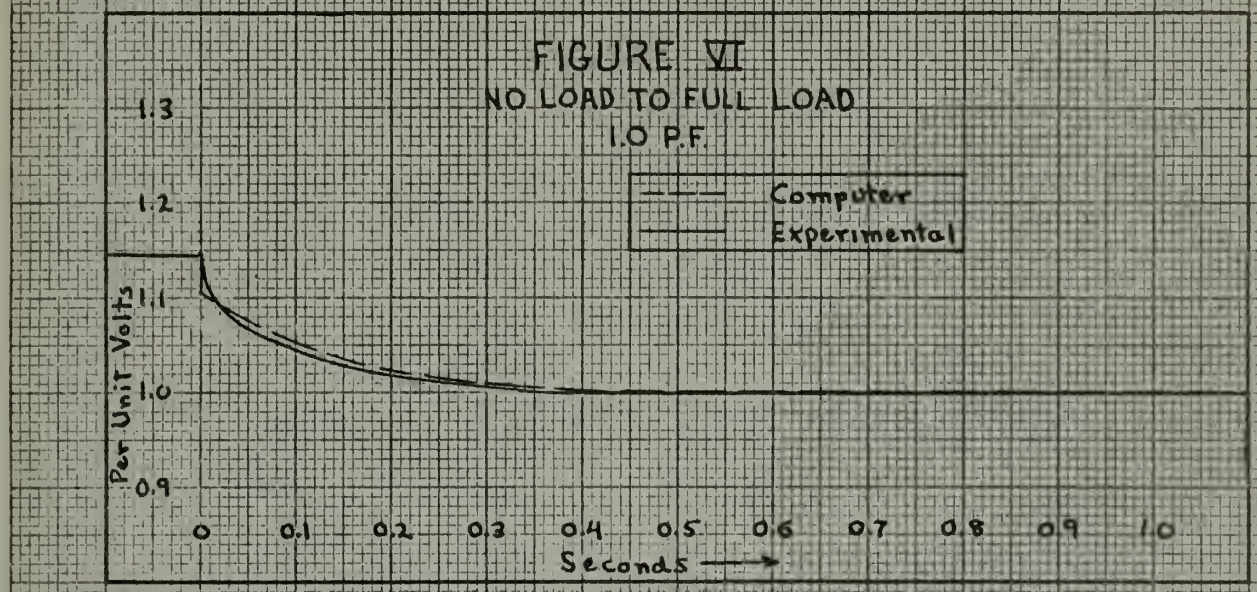

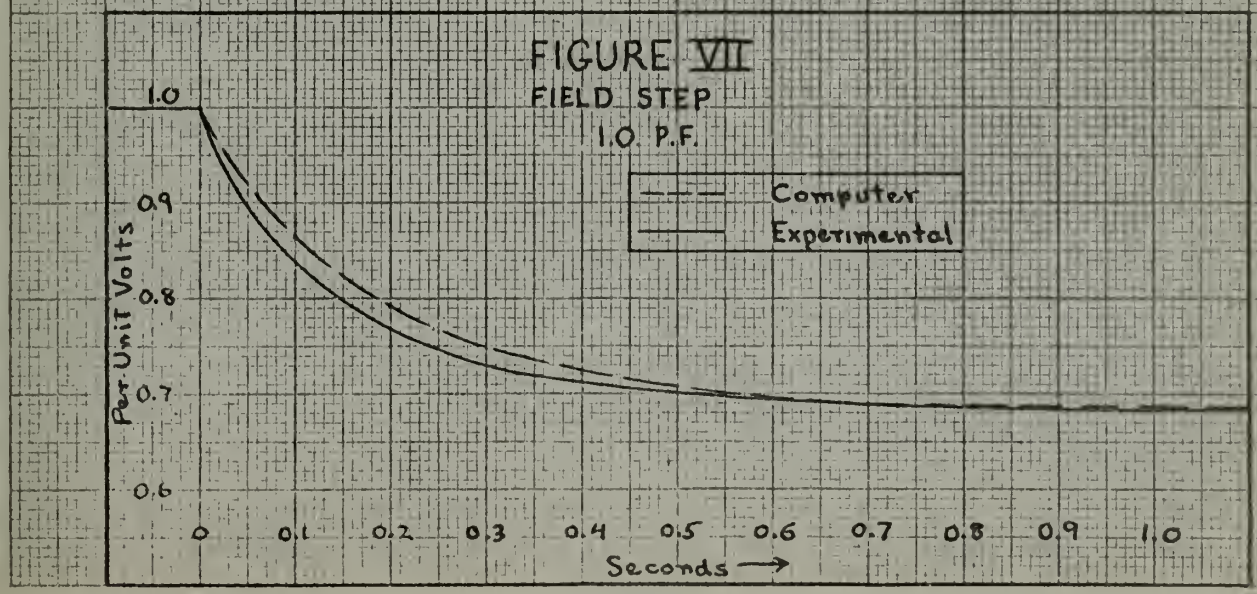

BAD-DBR
MAY '55

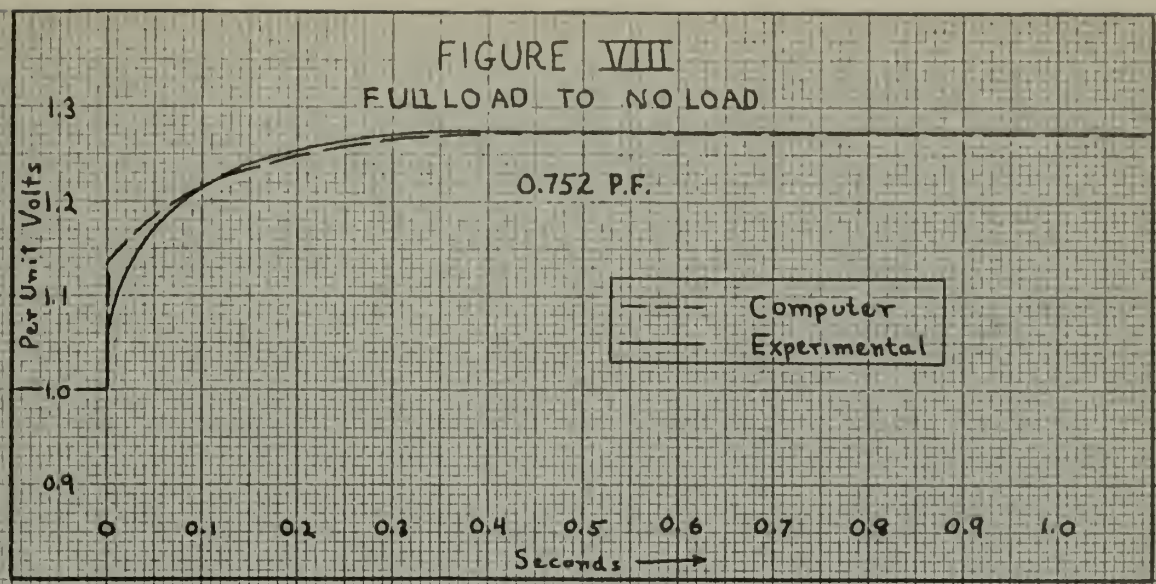

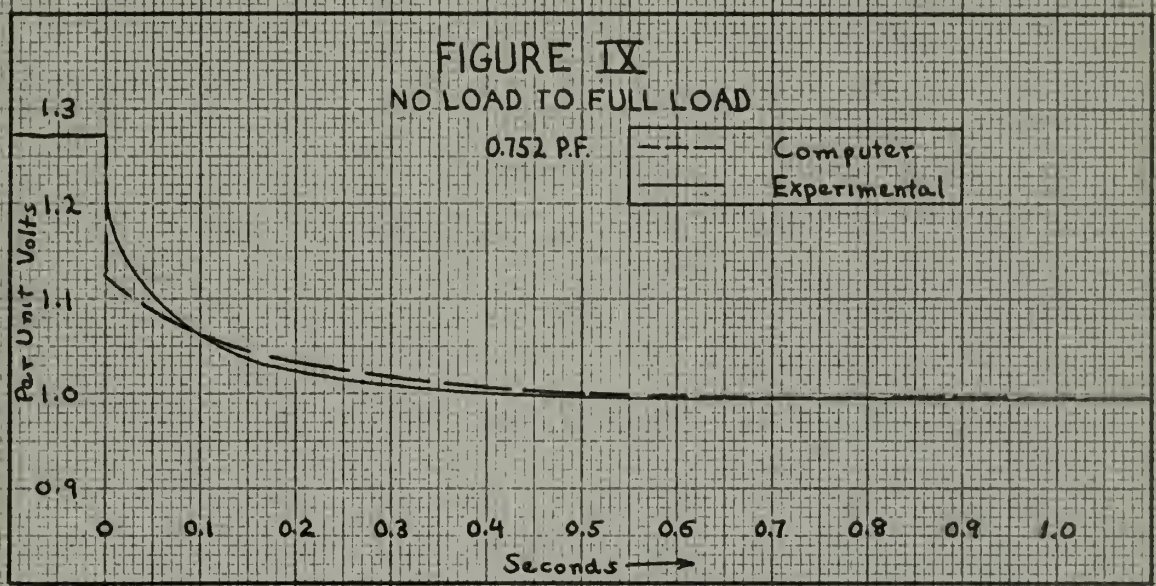

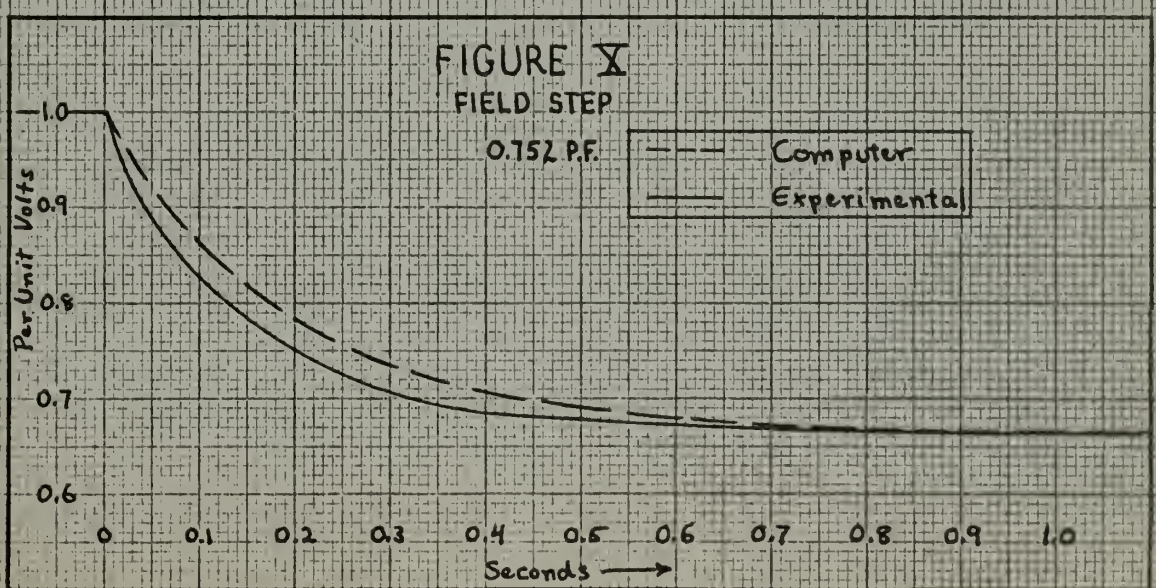

RAD-DBR
MAY '55

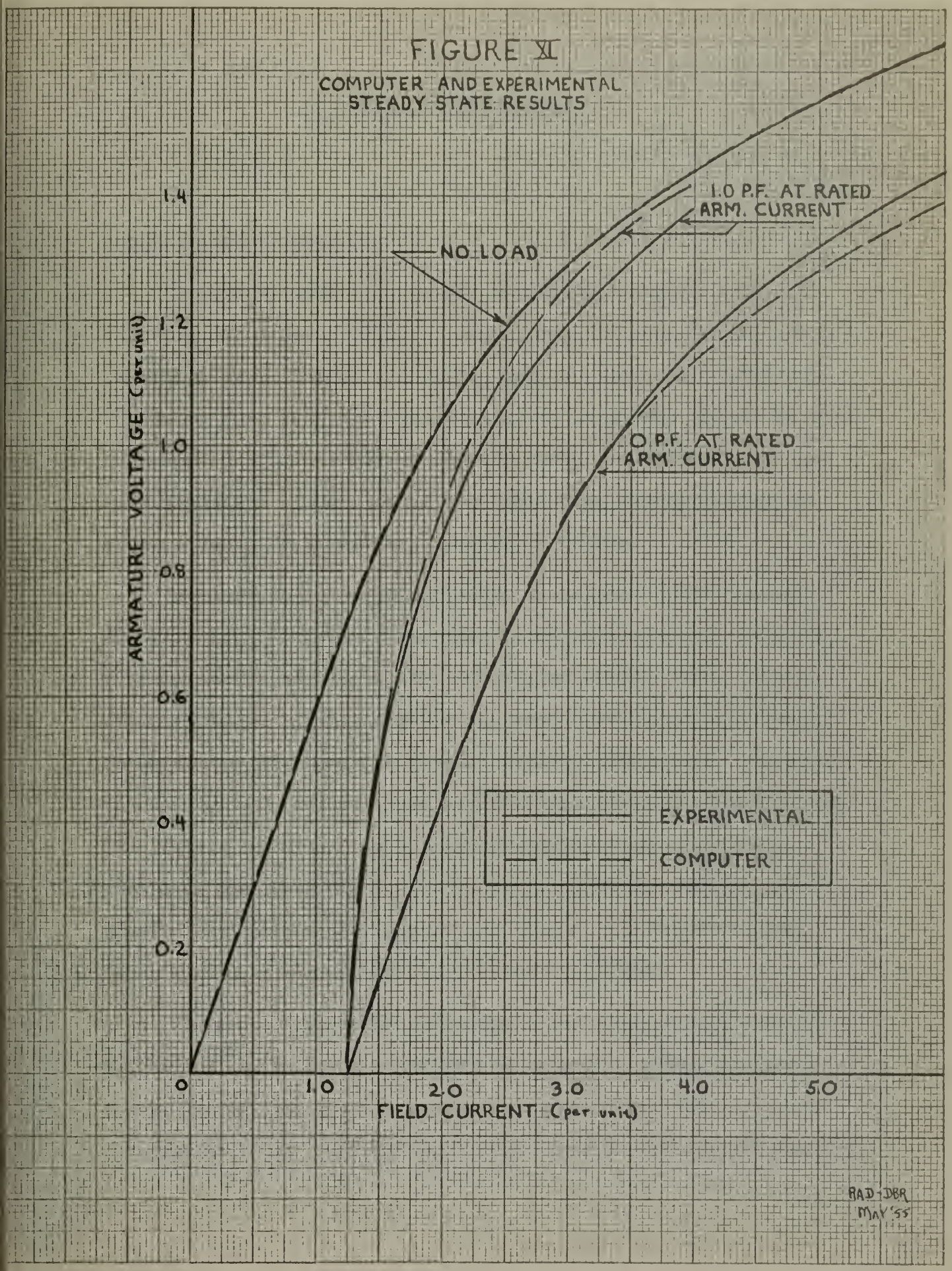
FIGURE XI
COMPUTER AND EXPERIMENTAL
STEADY STATE RESULTS
1.0 P.F. AT RATED
ARM. CURRENT
NO LOAD
0 P.F. AT RATED
ARM. CURRENT
EXPERIMENTAL
COMPUTER
ARMATURE VOLTAGE (per unit)
1.4
1.2
1.0
0.8
0.6
0.4
0.2
0
1.0
2.0
3.0
4.0
5.0
FIELD CURRENT (per unit)
RAD-DBR
MAY '55

IV

DISCUSSION OF RESULTS

Steady State Relationships

The no load saturation curves obtained by computer and experimental methods compared exactly over the entire range of field excitation used. This is as might be expected since the circuit at no load in the block diagram representation is completely defined by fixed quantities, i.e., the nonlinear characteristic, the field voltage, and field impedance. Thus, the no load correlation merely verifies the construction of the nonlinear characteristic curve.

The zero power factor saturation curves for both the computer and experimental studies were found to compare exactly as field current was increased until a point was reached slightly above rated armature voltage. At that point the computer curve began falling below the experimental curve with slowly increasing divergence. The analytical (computer) representation was developed assuming that the armature leakage reactance was a constant quantity equal to the Potier reactance (see Appendix C). Thus, the same Potier triangle moved parallel to itself would fit between the open circuit and zero power factor curves throughout the range of field excitation.

The zero power factor saturation curve does not have exactly the same shape as the open circuit characteristic shifted downward and to the right by constant amounts. The principal reason for this discrepancy is that the field leakage flux is not a constant under varying

conditions of loading. At zero power factor and with higher field excitations than those required for rated armature voltage, the field current is greater than for the same armature voltage on open circuit. This causes a higher field leakage flux and increased saturation due to the main air gap flux and the field leakage flux. This effectively causes the armature leakage reactance drop to be somewhat less than the Potier reactance. In general, the presence of field leakage in a salient pole machine causes the open circuit and load characteristic curves to draw near each other vertically for high values of saturation. This subject is covered with considerable clarity by Fitzgerald and Kingsley (see reference 4).

The correlation between the unity power factor saturation curves obtained experimentally and by computer is fairly close, agreeing exactly in the lower linear regions and diverging somewhat with increasing values of saturation. The computer curve gives higher armature voltage than the experimental curve at the same field excitation when in the saturated region. This discrepancy is largely due to the assumption of no saturation of magnetic material in the quadrature axis. This assumption is not entirely correct, but because the interpolar air gap spaces have such a high proportion of air in the magnetic circuit as compared to that in the direct axis magnetic circuit, the value of quadrature axis synchronous reactance, X_q, was assumed constant and unsaturated. Actually, some degree of saturation does exist at higher values of field excitation due to the presence of iron in the quadrature axis magnetic circuit, although not as much as in the direct axis. The effect of quadrature axis saturation is to reduce the value of X_q from its unsaturated value. Since the direct axis terminal

voltage, e_d, is directly proportional to X_q, saturation has the effect of reducing e_d and, consequently, the terminal voltage. Thus, the experimental saturation curve for unity power factor would rightly be expected to be lower than the corresponding computer curve.

It should be noted that while the computer characteristic for unity power factor is higher than the unity power factor experimental curve, the reverse is true for zero power factor loads as earlier explained. This is evident from a study of figure XI of the results. It therefore appears quite likely, that at some intermediate power factor between zero and unity, the variation of the analytic steady state values from those experimentally determined would be zero. For such a power factor the effect of decreasing field reactance with saturation would be cancelled by the decreasing value of X_q with saturation.

It would be possible to reduce the discrepancy between computer and experimental curves at unity power factor by inserting a saturation factor at X_q in the block diagram of figure I of the section on results to account for the discrepancy which presently exists. Further compensation to account for the small discrepancy between the computer and experimental zero power factor curves could also be accomplished by insertion of a nonlinear factor at the location of X_{al}. The resulting block diagram would give more accurate analytic results but would involve three nonlinear elements which are characteristic of a single machine. The relative simplicity of the representation developed in this thesis would have to be sacrificed to some degree in order to obtain a closer correlation between the experimental and analytic results.

Transient Relationships

Figures II through X of the section on results graphically compares the transient phenomena observed for the experimental and computer studies. The comparisons for full load to no load and for no load to full load are quite excellent. The transients in the terminal voltage due to a field step are also good, although not agreeing as closely as for the load changes.

The experimental transient is really a three time constant curve, one due to field transients, another due to armature transients, and the third due to subtransient effects of the amortisseur. The subtransient component of the experimental wave is of very short duration as compared with that portion caused by the field transient. Likewise, the armature transient is of short duration as compared to the field transient. The alternator block diagram as developed in this thesis has neglected the effects of the subtransient and armature transient components (see Appendix B). A study of the transients due to load changes in figures II through X shows the discrepancy between computer and experimental curves caused by neglecting these components. Their presence can only be noted for a short interval following the initiation of the transients, and they have completely disappeared after 0.1 seconds. After their disappearance, the experimental transient closely follows the computer transient. This result justifies the assumption that the alternator behaves like a single time constant machine.

In each of the nine transient comparisons the time constant associated with the experimental transient was somewhat less than the computer time constant. The best explanation for this consistent

error is that the measured value of field leakage reactance, X_{fl}, was probably in error since this was the least reliable parameter measurement. It was obtained by first measuring the time constant of the field transient associated with a step in field voltage with open circuit armature terminals. The time constant was then multiplied by the field resistance to obtain the field inductance. The leakage term was obtained by subtracting the mutual inductance term, common to both field and armature, from the value of field inductance. Thus, the field leakage inductance was the difference between two values close in magnitude and, hence, in subject to considerable error. A smaller value of field leakage inductance would decrease the computer time constant and make its transient approach the experimental transient.

The discrepancies occurring between computer and experimental transients for field steps were greater than for load changes. This was probably due to the method used for applying the field steps. In order to avoid changing the field resistance, the step was applied by shifting the excitation voltage source of 112 volts D.C. to another voltage source of approximately 70 volts D.C. A double throw switch was employed for this purpose. The switching delay was about 0.02 seconds during which time the excitation voltage was zero. Thus, during the delay period, the armature voltage was dropping toward zero as a final asymptote. The resulting experimental transient thus dropped more rapidly than would be the case if no switching delay were introduced.

The block diagram developed in this thesis does not account for changes in speed. As was previously explained, the initial or

final values of the experimental transients were adjusted in each case where they were graphically compared with the computer transients. In general, any change in load or excitation will cause a generator speed variation. These speed changes should be incorporated into the block diagram representation in order to extend its employment in the study of the voltage regulation problem. A method to properly account for speed in the alternator representation should be a subject for further study.

The final representation was developed assuming balanced load conditions. Any study of the voltage regulation problem should consider unbalanced load conditions due to faults in a single phase of the generator load. Thus, an additional recommendation for further investigation would be to study the possibility of including unbalanced loads in the generator-load representation.

V

CONCLUSIONS

(1) The block diagram development obtained in this thesis is a valid representation of the synchronous alternator. This conclusion is based on the close correlation obtained between the computer and experimental results in both the transient and steady states.

(2) The block diagram representation is a comparatively simplified form. This simplification results in some slight departures from actual steady state values in the saturated regions of the magnetization curve.

(3) At unity power factor, the computer steady state characteristic lies above the experimental curve. At zero power factor, the computer characteristic lies below the experimental curve. At load power factors intermediate between zero and one, the discrepancy between actual and analytic results would probably be less than the maximum error obtained at either 0 P. F. or 1.0 P. F. Since the normal load on a generator is rarely at either of these extremes, the resulting correlation of computer and experimental steady state data utilizing the alternator representation herein presented should be better than that obtained for either unity or zero power factors.

VI

RECOMMENDATIONS

(1) Investigation of methods to reduce the steady state errors at high values of field excitation with both zero and unity power factor loads.

(2) Investigation of the plausibility of including the effects of armature transients and amortisseur subtransients in the alternator block diagram.

(3) Study of a method to properly account for speed variations in the representation.

(4) Study of inclusion of unbalanced loads in the generator-load representation.

VII

APPENDIX

APPENDIX A

DEVELOPMENT OF THE LINEAR VOLT-AMPERE EQUATIONS DESCRIBING THE SYNCHRONOUS ALTERNATOR

Introduction

In the development of the volt-ampere equations for the synchronous alternator the methods outlined in reference 10 have been followed. The equations are first developed assuming motor action and utilizing the machine structure of figure I.

FIGURE (I)

Physical Structure of Machine

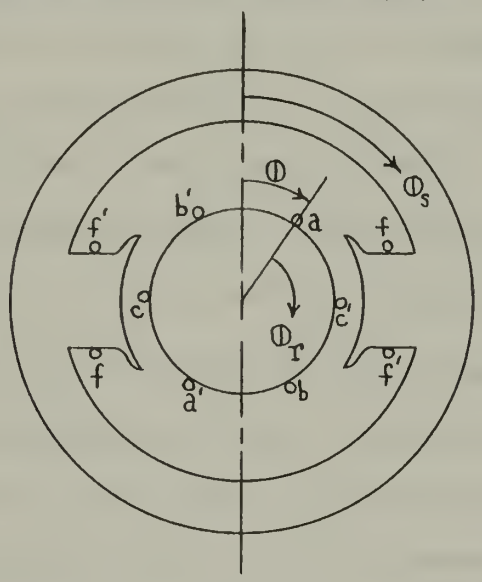

$$\Phi_s = \Phi + \Phi_r$$

Figure (I) places the salient field pole structure on the stator although in practice the d. c. field is usually placed on the rotor. Since relative motion is the only consideration, this representation is valid. However, in order to conform to standard synchronous generator practice, the equations will later be changed to show generator action and the salient field structure on the rotor.

The development below also makes the following assumptions:

(1) Geometrical symmetry exists on at least one side of the air gap.

(2) No slot openings exist.

(3) No saturation occurs.

(4) Sinusoidal mutual air gap flux density exists.

(5) Amortisseur windings are neglected.

Assumption (1) is valid since the machine tested has a cylindrical stator structure. Assumptions (2) and (3) are approximations which will be used in this portion of the report in order to develop linear differential equations with constant coefficients. Appendix B describes the method for the introduction of the nonlinear effects of saturation. Assumption (4) is a series approximation which is used even though the rotor of the machine tested is a salient member; this approximation can only be justified by the results obtained. For the machine tested, assumption (5) is not valid and is only used in order to simplify the analysis. In order to include these windings in the analysis it is necessary to add a second winding on the stator member of figure (I).

The development to be presented also assumes that the machine equations can be derived from linear lumped circuits in relative motion. Therefore, the three phase belts of the armature are replaced by three coils each of N equivalent turns which are sinusoidally distributed in space. Matrix algebra is used to aid in the development of the equations and reference 10 has been used throughout as a guide.

Phase Components

The electrical equations of motion for the salient pole machine

of figure (I) in terms of the phase variables are

$$\begin{bmatrix} \mathcal{V}^{s}_{n} \\ \hline \mathcal{V}^{r}_{m} \end{bmatrix} = \left[\begin{array}{c|c} \mathcal{R}^{ss}_{nn} + p\mathcal{L}^{ss}_{nn} & p\mathcal{L}^{sr}_{nm} \\ \hline p\mathcal{L}^{rs}_{mn} & \mathcal{R}^{rr}_{mm} + p\mathcal{L}^{rr}_{mm} \end{array}\right] \begin{bmatrix} \mathcal{I}^{s}_{n} \\ \hline \mathcal{I}^{r}_{m} \end{bmatrix} \tag{1}$$

where

$$\mathcal{R}^{ss}_{nn} = R_f \tag{2}$$

$$\mathcal{L}^{ss}_{nn} = L_f \tag{3}$$

$$\mathcal{R}^{rr}_{mm} = \begin{bmatrix} R^{rr}_{aa} & 0 & 0 \\ 0 & R^{rr}_{bb} & 0 \\ 0 & 0 & R^{rr}_{cc} \end{bmatrix} = \begin{bmatrix} R^{r} & 0 & 0 \\ 0 & R^{r} & 0 \\ 0 & 0 & R^{r} \end{bmatrix} \tag{4}$$

$$\mathcal{L}^{rr}_{mm} = \begin{bmatrix} L^{r}_{a} & -L^{r}_{b} & -L^{r}_{b} \\ -L^{r}_{b} & L^{r}_{a} & -L^{r}_{b} \\ -L^{r}_{b} & -L^{r}_{b} & L^{r}_{a} \end{bmatrix} + L^{r}_{c} \begin{bmatrix} \cos 2\emptyset & \cos(2\emptyset + d) & \cos(2\emptyset + 2d) \\ \cos(2\emptyset + d) & \cos(2\emptyset + 2d) & \cos 2\emptyset \\ \cos(2\emptyset + 2d) & \cos 2\emptyset & \cos(2\emptyset + d) \end{bmatrix} \tag{5}$$

$$L^{r}_{a} = K\pi \frac{N^2}{2} p_o \tag{6}$$

$$-L^{r}_{b} = K\pi \frac{N^2}{2} p_o \cos d = K\pi \frac{N^2}{2} p_o \cos 2d \tag{7}$$

$$-L^{r}_{c} = K\pi \frac{N^2}{2} \frac{p_2}{2} \tag{8}$$

air gap permeance, $p = p_o + p_2 \cos 2\emptyset_s + p_4 \cos 4\emptyset_s + ---$

$$= p_o + p_2 \cos 2(\emptyset^r + \emptyset) \tag{9}$$

$$\mathcal{L}^{sr}_{nm} = \left[L_f L_a / L_f L_b / L_f L_c\right] = M\left[\cos\phi / \cos(\phi + d) / \cos(\phi + 2d)\right] \tag{10}$$

$$\mathcal{L}^{rs}_{mn} = \left[\mathcal{L}^{sr}_{nm}\right]^t = M\begin{bmatrix}\cos\phi \\ \cos(\phi + d) \\ \cos(\phi + 2d)\end{bmatrix} \tag{11}$$

$$\mathcal{V}^s_n = V_f \;;\; \mathcal{I}^s_n = I_f \;;\; \mathcal{V}^r_m = \begin{bmatrix}V_a \\ V_b \\ V_c\end{bmatrix} \;;\; \mathcal{I}^r_m = \begin{bmatrix}I_a \\ I_b \\ I_c\end{bmatrix} \tag{12}$$

Finally, in terms of the phase components the equations become

$$\begin{bmatrix}V_a \\ V_b \\ V_c \\ \hline V_f\end{bmatrix} = \left[\begin{array}{ccc:c}
R^r + p\left[L_a + L_c\cos 2\phi\right] & p\left[-L_b + L_c\cos(2\phi + d)\right] & p\left[-L_b + L_c\cos(2\phi + 2d)\right] & M\cos\phi \\
p\left[-L_b + L_c\cos(2\phi + d)\right] & R^r + p\left[L_a + L_c\cos(2\phi + 2d)\right] & p\left[-L_b + L_c\cos 2\phi\right] & M\cos(\phi + d) \\
\hdashline
M\cos\phi & M\cos(\phi + d) & M\cos(\phi + 2d) & R_f + pL_f
\end{array}\right] \cdot \begin{bmatrix}I_a \\ I_b \\ I_c \\ \hline I_f\end{bmatrix} \tag{13}$$

Symmetrical Components

In order to simplfy the equations, the Lyon transformation is used to obtain symmetrical components. To accomplish this simplification, use is made of the transformations

$$\mathcal{A} = \frac{1}{3}\begin{bmatrix}1 & 1 & 1 \\ 1 & a & a^2 \\ 1 & a^2 & a\end{bmatrix} \quad \text{where } a = e^{j(2\pi/3)} \tag{14}$$

and

$$\mathcal{A}^{-1} = \begin{bmatrix} 1 & 1 & 1 \\ 1 & a^2 & a \\ 1 & a & a^2 \end{bmatrix} \tag{15}$$

and the voltages, currents, and impedance are converted to symmetrical components as follows:

$$\mathcal{V}^s_N = \mathcal{V}^s_n = V_f \tag{16}$$

$$\mathcal{I}^s_N = \mathcal{I}^s_n = I_f \tag{17}$$

$$\mathcal{V}^r_M = \mathcal{A}\mathcal{V}^r_m = \begin{bmatrix} V_o \\ V_+ \\ V_- \end{bmatrix} = \frac{1}{3}\begin{bmatrix} (V_a + V_b + V_c) \\ (V_a + a\,V_b + a^2\,V_c) \\ (V_a + a^2\,V_b + a\,V_c) \end{bmatrix} \tag{18}$$

$$\mathcal{I}^r_M = \mathcal{A}\mathcal{I}^r_m = \begin{bmatrix} I_o \\ I_+ \\ I_- \end{bmatrix} = \frac{1}{3}\begin{bmatrix} (I_a + I_b + I_c) \\ (I_a + a\,I_b + a^2\,I_c) \\ (I_a + a^2\,I_b + a\,I_c) \end{bmatrix} \tag{19}$$

$$\mathcal{Z}^{sr}_{NM} = \left[\begin{array}{c|c} \mathcal{R}^{rr}_{MM} + p\,\mathcal{L}^{rr}_{MM} & p\,\mathcal{L}^{rs}_{MN} \\ \hline p\,\mathcal{L}^{sr}_{NM} & \mathcal{R}^{ss}_{NN} + p\,\mathcal{L}^{ss}_{NN} \end{array}\right]$$

$$= \left[\begin{array}{c|c} \mathcal{A}(\mathcal{R}^{rr}_{mm} + p\,\mathcal{L}^{rr}_{mm})\mathcal{A}^{-1} & \mathcal{A}\,p\,\mathcal{L}^{rs}_{mn} \\ \hline p\,\mathcal{L}^{sr}_{nm}\mathcal{A}^{-1} & \mathcal{R}^{ss}_{nn} + p\,\mathcal{L}^{ss}_{nn} \end{array}\right] \tag{20}$$

$$\mathcal{R}^{rr}_{MM} = \mathcal{A}\begin{bmatrix} R^r & 0 & 0 \\ 0 & R^r & 0 \\ 0 & 0 & R^r \end{bmatrix}\mathcal{A}^{-1} = \begin{bmatrix} R^r & 0 & 0 \\ 0 & R^r & 0 \\ 0 & 0 & R^r \end{bmatrix} \tag{21}$$

$$\mathcal{L}^{rr}_{MM} = \mathcal{A}\left[\begin{bmatrix} L_a & -L_b & -L_b \\ -L_b & L_a & -L_b \\ -L_b & -L_b & L_a \end{bmatrix} + L_c \begin{bmatrix} \cos 2\phi & \cos(2\phi + d) & \cos(2\phi + 2d) \\ \cos(2\phi + d) & \cos(2\phi + 2d) & \cos 2\phi \\ \cos(2\phi + 2d) & \cos 2\phi & \cos(2\phi + d) \end{bmatrix}\right] \mathcal{A}^{-1}$$

$$= \begin{bmatrix} L_a - 2L_b & 0 & 0 \\ 0 & L_a + L_b & 3/2\, L_c\, e^{-j2\phi} \\ 0 & 3/2\, L_c\, e^{j2\phi} & L_a + L_b \end{bmatrix} \tag{22}$$

$$\mathcal{R}^{ss}_{NN} = \mathcal{R}^{ss}_{nn} = R_f \tag{23}$$

$$\mathcal{L}^{ss}_{NN} = \mathcal{L}^{ss}_{nn} = L_f \tag{24}$$

$$p\,\mathcal{L}^{sr}_{NM} = p\,\mathcal{L}^{sr}_{nm}\,\mathcal{A}^{-1} = p\,M\begin{bmatrix}\cos\phi & \cos(\phi + d) & \cos(\phi + 2d)\end{bmatrix}\mathcal{A}^{-1}$$

$$= p\,\frac{3}{2}\,M\begin{bmatrix}0 & e^{j\phi} & e^{-j\phi}\end{bmatrix} \tag{25}$$

$$p\,\mathcal{L}^{rs}_{MN} = \mathcal{A}\,p\,\mathcal{L}^{rs}_{mn} = \mathcal{A}\,p\,M\begin{bmatrix}\cos\phi \\ \cos(\phi + d) \\ \cos(\phi + 2d)\end{bmatrix} = \frac{p\,M}{2}\begin{bmatrix}0 \\ e^{-j\phi} \\ e^{j\phi}\end{bmatrix} \tag{26}$$

Combining equations (16) through (26) in order to obtain a complete volt-ampere equation in Lyon instantaneous symmetrical components,

$$\begin{bmatrix} V_o \\ V_+ \\ V_- \\ \hline V_f \end{bmatrix} = \left[\begin{array}{ccc|c} R^r + p(L_a - 2L_b) & 0 & 0 & 0 \\ 0 & R^r + p(L_a + L_b) & p\frac{3}{2} L_c\, e^{-j2\phi} & p\frac{M}{2} e^{-j\phi} \\ 0 & p\frac{3}{2} L_c\, e^{j2\phi} & R^r + p(L_a + L_b) & p\frac{M}{2} e^{j\phi} \\ \hline 0 & p\frac{3}{2} M\, e^{j\phi} & p\frac{3}{2} M\, e^{-j\phi} & R_f + p L_f \end{array}\right] \begin{bmatrix} I_o \\ I_+ \\ I_- \\ \hline I_f \end{bmatrix} \qquad (27)$$

Rotating Components

In order to obtain linear differential equations with constant coefficients the positional dependency must be removed and a speed dependency substituted. Then, if constant speed is assumed, the equations become linear. For a salient pole machine the necessary transformations can only be made by referring the symmetrical member to the salient member; in this instance this will mean that the rotor quantities will be referred to the stator. In equation (27) only the +, -, and field components are positionally dependent and torque-producing; therefore, only these components need to be transformed. In order to convert symmetrical components to rotating components the transformations shown in equation (28) will be used.

$$\mathcal{B} = \begin{bmatrix} e^{j\phi} & 0 & 0 \\ 0 & e^{-j\phi} & 0 \\ 0 & 0 & 1 \end{bmatrix} ; \qquad \mathcal{B}^{-1} = \begin{bmatrix} e^{-j\phi} & 0 & 0 \\ 0 & e^{j\phi} & 0 \\ 0 & 0 & 1 \end{bmatrix} \qquad (28)$$

With these transformations the voltages, currents, and impendances in rotating components become

$$\mathcal{V}^{sr}_{f,b} = \mathcal{B}\mathcal{V}^{sr}_{NM} \qquad \mathcal{I}^{sr}_{f,b} = \mathcal{B}\mathcal{I}^{sr}_{NM}$$

$$\mathcal{Z}^{sr}_{f,b} = \mathcal{B}\mathcal{Z}^{sr}_{NM}\mathcal{B}^{-1} \tag{29}$$

$$\begin{bmatrix} V_f \\ V_b \\ \hdashline V_{field} \end{bmatrix} = \mathcal{B}\left[\begin{array}{cc:c} R^r + p(L_a + L_b) & p\frac{3}{2}L_c e^{-j2\phi} & p\frac{M}{2}e^{-j\phi} \\ p\frac{3}{2}L_c e^{j2\phi} & R^r + p(L_a + L_b) & p\frac{M}{2}e^{j\phi} \\ \hdashline p\frac{3}{2}M e^{j\phi} & p\frac{3}{2}M e^{-j\phi} & R_f + pL_f \end{array}\right]\mathcal{B}^{-1} \cdot \begin{bmatrix} I_f \\ I_b \\ \hdashline I_{field} \end{bmatrix} \tag{30}$$

After completing the necessary matrix multiplications the completed equations in rotating components become

$$\begin{bmatrix} V_o \\ V_f \\ V_b \\ \hdashline V_{field} \end{bmatrix} = \left[\begin{array}{ccc:c} R^r + p(L_a - 2L_b) & 0 & 0 & 0 \\ 0 & R^r + (p - j\dot{\phi})(L_a + L_b) & \frac{3}{2}L_c(p - j\dot{\phi}) & \frac{M}{2}(p - j\dot{\phi}) \\ 0 & \frac{3}{2}L_c(p + j\dot{\phi}) & R^r + (p + j\dot{\phi})(L_a + L_b) & \frac{M}{2}(p + j\dot{\phi}) \\ \hdashline 0 & p\frac{3}{2}M & p\frac{3}{2}M & R_f + pL_f \end{array}\right] \begin{bmatrix} I_o \\ I_f \\ I_b \\ \hdashline I_{field} \end{bmatrix} \tag{31}$$

Park's Direct and Quadrature Two-Axis Components

Since the rotating components are speed dependent with rotor quantities referred to the stator, the real direct and quadrature two-axis components can be obtained directly from the complex rotating components by using the change of variable of equation (32).

$$\mathcal{A} = \begin{bmatrix} 1 & 0 & 0 \\ 0 & 1 & 1 \\ 0 & -j & j \end{bmatrix} \quad ; \quad \mathcal{A}^{-1} = \begin{bmatrix} 1 & 0 & 0 \\ 0 & \frac{1}{2} & j/2 \\ 0 & \frac{1}{2} & -j/2 \end{bmatrix} \tag{32}$$

The volt-ampere equation in two axis components becomes

$$\begin{bmatrix} \mathcal{A}\mathcal{V}^{r}_{f,b} \\ \mathcal{V}^{s}_{f,b} \end{bmatrix} = \begin{bmatrix} \mathcal{A}\mathcal{Z}^{rr}_{f,b}\mathcal{A}^{-1} & \mathcal{A}\mathcal{Z}^{rs}_{f,b} \\ \mathcal{Z}^{sr}_{f,b}\mathcal{A}^{-1} & \mathcal{Z}^{ss}_{f,b} \end{bmatrix} \begin{bmatrix} \mathcal{A}\mathcal{I}^{r}_{f,b} \\ \mathcal{I}^{s}_{f,b} \end{bmatrix} \tag{33}$$

where

$$\mathcal{A}\mathcal{Z}^{rr}_{f,b}\mathcal{A}^{-1} = \begin{bmatrix} R^r + p(L_a - 2L_b) & 0 & 0 \\ 0 & R^r + p(L_a + L_b + \frac{3}{2}L_c) & \dot{\phi}(L_a + L_b - \frac{3}{2}L_c) \\ 0 & -\dot{\phi}(L_a + L_b + \frac{3}{2}L_c) & R^r + p(L_a + L_b - \frac{3}{2}L_c) \end{bmatrix} \tag{34}$$

$$\mathcal{A}\mathcal{Z}^{rs}_{f,b} = \begin{bmatrix} 0 \\ M_p \\ -M\dot{\phi} \end{bmatrix} \tag{35}$$

$$\mathcal{Z}^{sr}_{f,b}\mathcal{A}^{-1} = \begin{bmatrix} 0 & p\frac{3}{2}M & 0 \end{bmatrix} \tag{36}$$

Combining the results of equations (34), (35), and (36), the completed equations in Park's two-axis components are

$$
\begin{bmatrix} V_o \\ V_d \\ V_q \\ \hline V_f \end{bmatrix} = \left[\begin{array}{ccc|c} R^r + p(L_a - 2L_b) & 0 & 0 & 0 \\ 0 & R^r + p(L_a + L_b + \frac{3}{2} L_c) & \dot{\phi}(L_a + L_b - \frac{3}{2} L_c) & M p \\ 0 & -\dot{\phi}(L_a + L_b + \frac{3}{2} L_c) & R^r + p(L_a + L_b - \frac{3}{2} L_c) & -M\dot{\phi} \\ \hline 0 & p\,\frac{3}{2} M & 0 & R_f + p L_f \end{array}\right] \begin{bmatrix} I_o \\ I_d \\ I_q \\ \hline I_f \end{bmatrix} \tag{37}
$$

Defining the direct axis and quadrature axis inductances as

$$
L_d = L_a + L_b + \frac{3}{2} L_c \qquad \text{and}
$$

$$
L_q = L_a + L_b - \frac{3}{2} L_c \tag{38}
$$

The equations for motor action and the physical structure of figure (I) become

$$
\begin{bmatrix} V_o \\ V_d \\ V_q \\ \hline V_f \end{bmatrix} = \left[\begin{array}{ccc|c} R^r + p(L_a - 2L_b) & 0 & 0 & 0 \\ 0 & R^r + p L_d & \dot{\phi} L_q & M p \\ 0 & -\dot{\phi} L_d & R^r + p L_q & -M\dot{\phi} \\ \hline 0 & p\,\frac{3}{2} M & 0 & R_f + p L_f \end{array}\right] \begin{bmatrix} I_o \\ I_d \\ I_q \\ \hline I_f \end{bmatrix} \tag{39}
$$

<u>Generator Equations</u>

The volt-ampere equations have been derived for motor action assuming clockwise rotation of the armature as indicated in figure (I).

In order to obtain generator equations the following changes must be made:

(1) Since the field (rotor) rotates in a clockwise direction, the armature must revolve counterclockwise or opposite to the direction shown in figure (I). Therefore, all speed terms in the matrix must have their signs changed.

(2) The matrix as given is developed in terms of voltage drops. In order for the equations to be in terms of generator voltage rises, all V terms must have their signs changed, i.e., e = -V.

(3) The electromagnetic torque for a motor is positive while for a generator it is negative. Since the sign of the torque is governed by the polarity of the excitation current, I_f must be made negative for a generator.

Making the changes indicated above, the volt-ampere matrix for a generator becomes

$$\begin{bmatrix} e_o \\ e_d \\ e_q \\ \hline e_f \end{bmatrix} = \left[\begin{array}{ccc|c} -R^r - p(L_a - 2L_b) & 0 & 0 & 0 \\ 0 & -R^r - pL_d & \dot{\phi} L_q & Mp \\ 0 & -\dot{\phi} L_d & -R^r - pL_q & M\dot{\phi} \\ \hline 0 & -p\frac{3}{2}M & 0 & R_f + pL_f \end{array}\right] \begin{bmatrix} I_o \\ I_d \\ I_q \\ \hline I_f \end{bmatrix} \qquad (40)$$

Thus, the linear volt-ampere equations describing the synchronous alternator in Park's d-q two-axis components become

$$e_d = -(R^r + pL_d)I_d + \dot{\phi} L_q I_q + Mp\, I_f \qquad (41)$$

$$e_q = -\dot{\phi} L_d I_d - (R^r + p L_q) I_q + M \dot{\phi} I_f \tag{42}$$

$$e_f = -p \frac{3}{2} M I_d + (R_f + p L_f) I_f \tag{43}$$

APPENDIX B

DEVELOPMENT OF A COMPUTER BLOCK DIAGRAM REPRESENTATION OF THE SYNCHRONOUS ALTERNATOR AND ITS CONNECTED LOAD, INCLUDING EFFECTS OF NONLINEARITIES

Development of Linear Block Diagram

The linear differential equations derived in Appendix A for a salient pole synchronous generator with resistive-inductive loading are

$$e_d = -(R + pL_d) + \phi L_q I_q + M_p I_f \tag{1}$$

$$e_q = -\dot{\phi} L_d I_d - (R + pL_q) I_q + M\dot{\phi} I_f \tag{2}$$

$$e_f = -p\,\frac{3}{2}\,M I_d + (R_f + pL_f) I_f \tag{3}$$

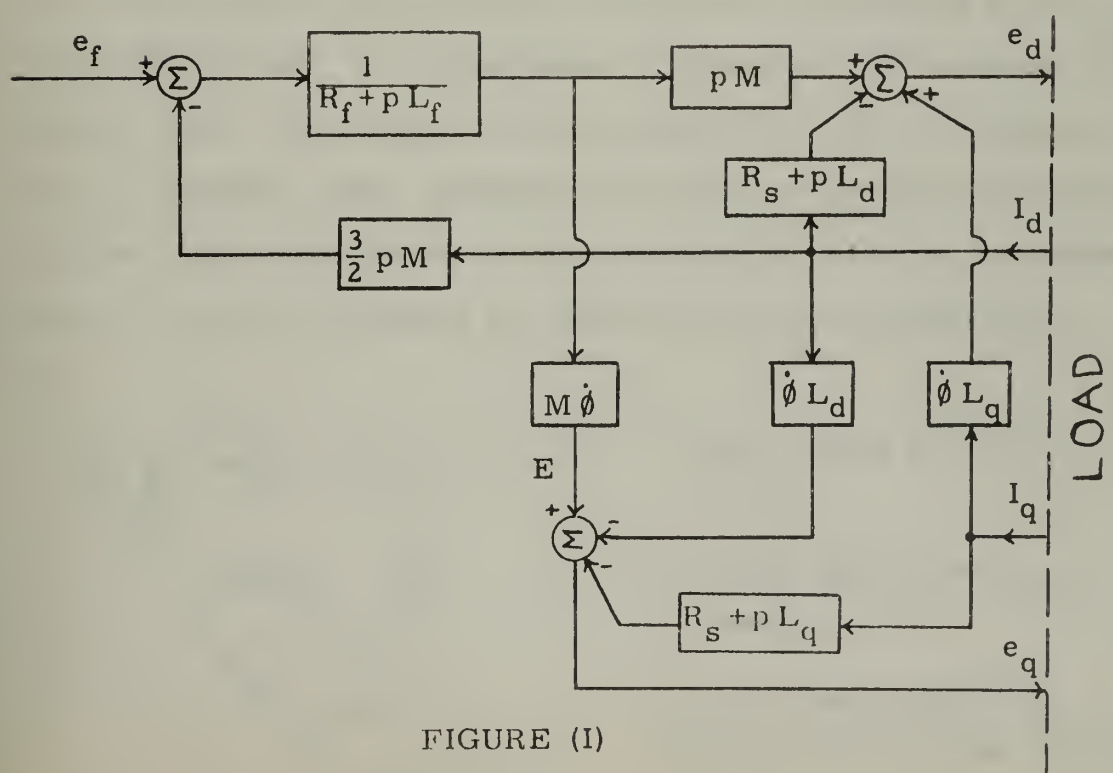

FIGURE (I)

These equations can be represented by a block diagram in which e_f is the exciting signal and the direct and quadrature currents and voltages feed a load as yet undefined.

The block diagram obtained above is derived from equations which do not account for the subtransient effects due to the amortisseur. These subtransients are of very short duration compared to others which are present, and it is often justified to neglect them in considering the problems of voltage regulation and system design.

It should be noted that e_d, e_q, i_d, and i_q are actually direct current modulating envelopes of an A. C. carrier. Variation in these quantities occur only transientwise.

The equations representing the load to be applied to the generator terminals can be obtained in a straightforward manner from a study of the vector diagram describing the volt-ampere relationship of the load in the steady state. The steady state relationship is not an exact relationship, since any changes in the load signal will cause transients to occur. However, these transients, which are unidirectional, do not produce appreciable effects and hence are neglected in the same manner that the armature transients are neglected as will be shown later.

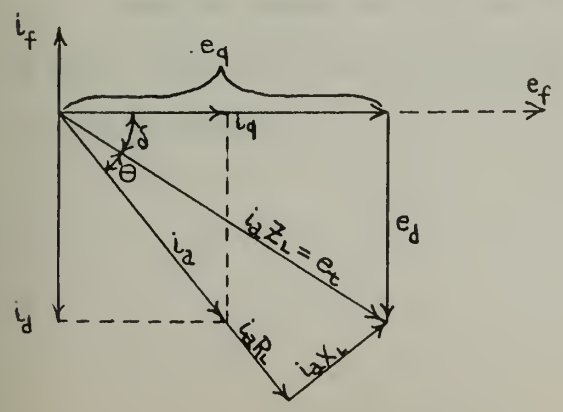

FIGURE (II)

θ = phase angle between i_a and e_t

δ = power angle between e_t and e_f

X_L, R_L, and Z_L are the absolute values of load impedance

$$i_d = i_a \sin(\delta + \theta) \qquad (4d) \qquad\qquad i_q = i_a \cos(\delta + \theta) \qquad (4q)$$

also:

$$e_d = e_t \sin\delta = i_a Z_L \sin\delta \qquad (5d) \qquad\qquad e_q = e_t \cos\delta = i_a Z_L \cos\delta \qquad (5q)$$

$$\therefore\ i_a = \frac{e_d}{Z_L \sin\delta} \qquad (6d) \qquad\qquad \therefore\ i_a = \frac{e_q}{Z_L \cos\delta} \qquad (6q)$$

Substituting equation (6) into equation (4),

$$i_d = \frac{e_d}{Z_L \sin\delta} \sin(\delta + \theta) \qquad\qquad i_q = \frac{e_q}{Z_L \cos\delta} \cos(\delta + \theta)$$

$$= \frac{e_d}{Z_L \sin\delta} \left[\sin\delta \cos\theta + \sin\theta \cos\delta\right] \qquad\qquad = \frac{e_q}{Z_L \cos\delta} \left[\cos\delta \cos\theta - \sin\delta \sin\theta\right]$$

$$= \frac{e_d}{Z_L} \left[\cos\theta + \sin\theta \cot\delta\right] \qquad (7d) \qquad\qquad = \frac{e_q}{Z_L} \left[\cos\theta - \sin\theta \tan\delta\right] \qquad (7q)$$

$$\text{but} \quad \cot\delta = \frac{e_q}{e_d} \qquad (8d) \qquad\qquad \tan\delta = \frac{e_d}{e_q} \qquad (8q)$$

Therefore

$$i_d = \frac{e_d}{Z_L} \cos\theta + \frac{e_q}{Z_L} \sin\theta \qquad (9d) \qquad\qquad i_q = \frac{e_q}{Z_L} \cos\theta - \frac{e_d}{Z_L} \sin\theta \qquad (9q)$$

Applying equations (9d) and (9q), the load can now be represented in block diagram form and added to the block diagram earlier obtained for the generator.

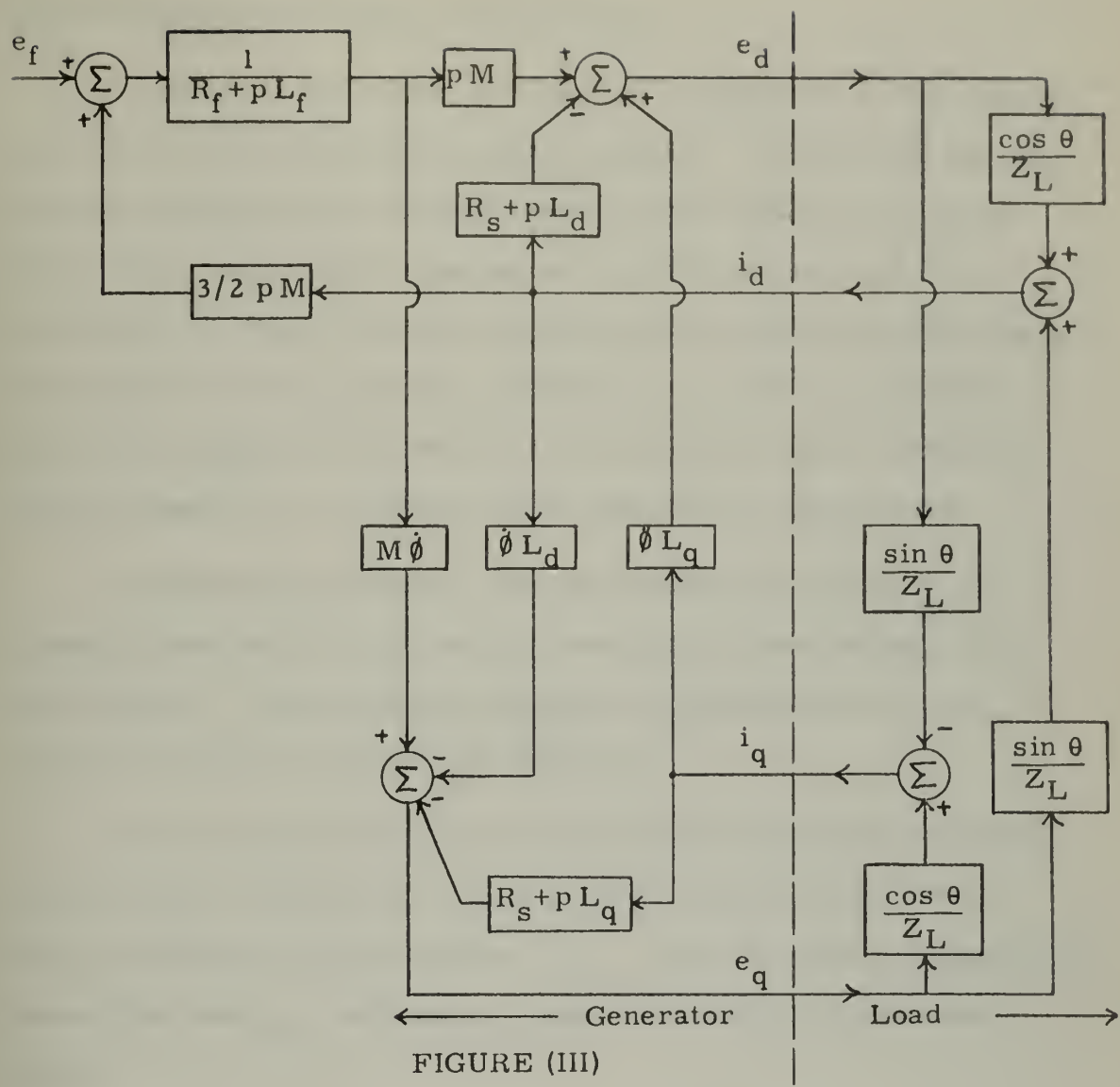

FIGURE (III)

Basic Assumptions

The block diagram represented above does not account for the saturation effects normally encountered in a magnetic circuit. To account for the saturation of the machine, the nonlinearity is approximated by means of a single characteristic which can be placed in such a position in the block diagram as to correct for the linear,

characteristic block diagram obtained above.

In addition to neglecting subtransient components, it can also be seen that armature transients can be neglected. These transients are largely responsible for a second harmonic wave which is not detectable on the experimental transient current wave forms, and also account for the direct current transients of the output wave which vary from phase to phase depending upon the time in each cycle at which the transient signal is introduced. It would thus be quite difficult to compare these D. C. transients experimentally and analytically.

An acceptable procedure is to neglect them since they do not produce appreciable effects upon the average terminal voltage of the three phases. This assumption amounts to dropping the pL_d, pL_q, and the pM terms from the block diagram.

In a salient pole machine, the reactance of direct axis armature reaction, X_{ad}, saturates to a much greater extent than the corresponding quadrature axis reactance, X_{aq}. It is, therefore, a reasonable assumption that X_{aq}, and thus L_q, does not saturate, but remains linear.

Two final assumptions are that the armature resistance is negligible, and that the speed remains constant corresponding to an electrical frequency of 60 cps.

Per Unit System

In order to simplify the linear block diagram so as to more easily handle saturation effects, a per unit system will be used as here

defined. The stator quantities based on machine rating are defined as:

BASE ARMATURE QUANTITIES

e_{ao} = rated peak phase voltage

i_{ao} = rated peak phase current

$X_{ao} = \omega L_{ao} = e_{ao}/i_{ao}$ = armature base reactance

$$X_d = \frac{L_d}{L_{ao}} \qquad X_q = \frac{L_q}{L_{ao}}$$

$$X_{ad} = \frac{L_{ad}}{L_{ao}}$$

The per unit system as now defined for the rotor circuit is a reciprocal system in which the base field current is the field current which will induce in each stator phase a voltage equal to $X_{ad}\, i_{ao}$. (8) The per unit impedances of the elements in the rotor circuit (field circuit) are obtained by transferring the corresponding physical impedances to the stator by an effective stator-rotor turn ratio, and dividing the transferred values by X_{ao}. This makes $X_{mf} = X_{ad} = X_{af} = X_{md}$ in the per unit system. Thus, the following per unit field quantities can be defined:

i_{fo} = that field current which is read directly on the air-gap line of the no-load saturation curve corresponding to a per unit armature voltage equal to per unit X_{ad}

$$e_f = \frac{e_f}{e_{ao}} \left(\frac{i_{fo}}{3/2\, i_{ao}}\right)$$

$$X_{md} = \frac{3}{2} \frac{M}{L_{ao}} \left(\frac{i_{fo}}{3/2\, i_{ao}}\right)$$

$$X_{mf} = \frac{3}{2} \frac{L_f}{L_{ao}} \left(\frac{i_{fo}}{3/2\, i_{ao}}\right)^2$$

$$R_f = \frac{3}{2}\frac{R_f}{X_{ao}}\left(\frac{i_{fo}}{3/2\, i_{ao}}\right)^2$$

per unit $\dot{\phi}$ = 1 at rated speed

$$p = \text{per unit time differential operator} = \frac{d}{d\omega_o t}$$

Block Diagram Including Nonlinear Effects

If the block diagram parameters are expressed in the per unit reciprocal system as defined in the preceding section, and the assumptions of Section II are applied, equations (1), (2), and (3) can be written.

$$e_d = X_{aq} I_q \tag{10}$$

$$e_q = X_{md} I_f - (X_{al} + X_{md}) I_d \tag{11}$$

$$e_f = (R_f + p X_{md}) I_f - p X_{md} I_d \tag{12}$$

The effect of saturation is introduced in a single characteristic which effectively converts an open circuit voltage to a linearized air gap voltage. This introduction of the nonlinearity is accomplished by changing from the open circuit field current to a hypothetical air gap current as shown below.

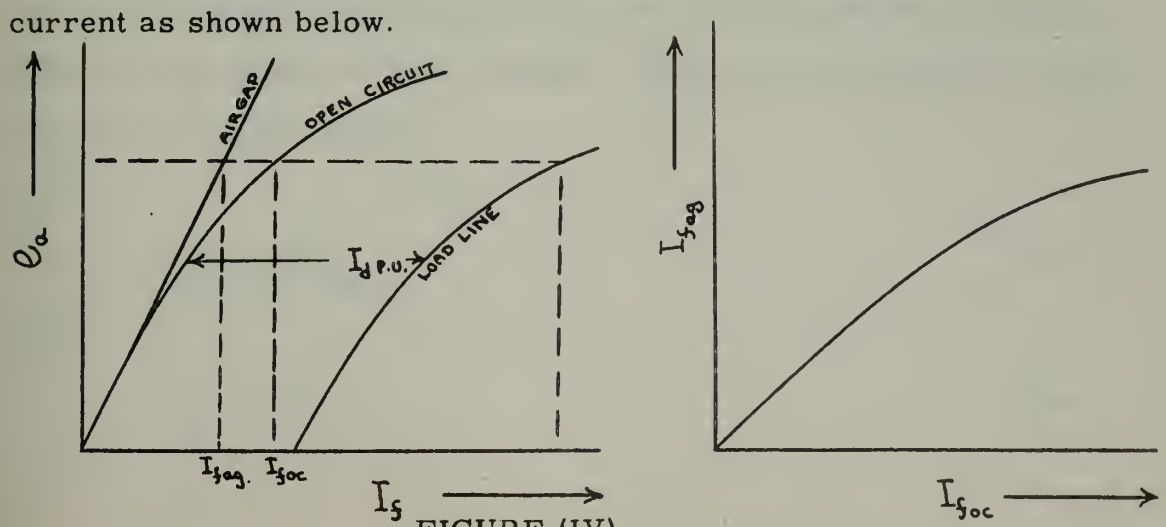

FIGURE (IV)

The complete block diagram which accounts for saturation of the magnetizing circuit (assuming X_q linear) is given below in per unit.

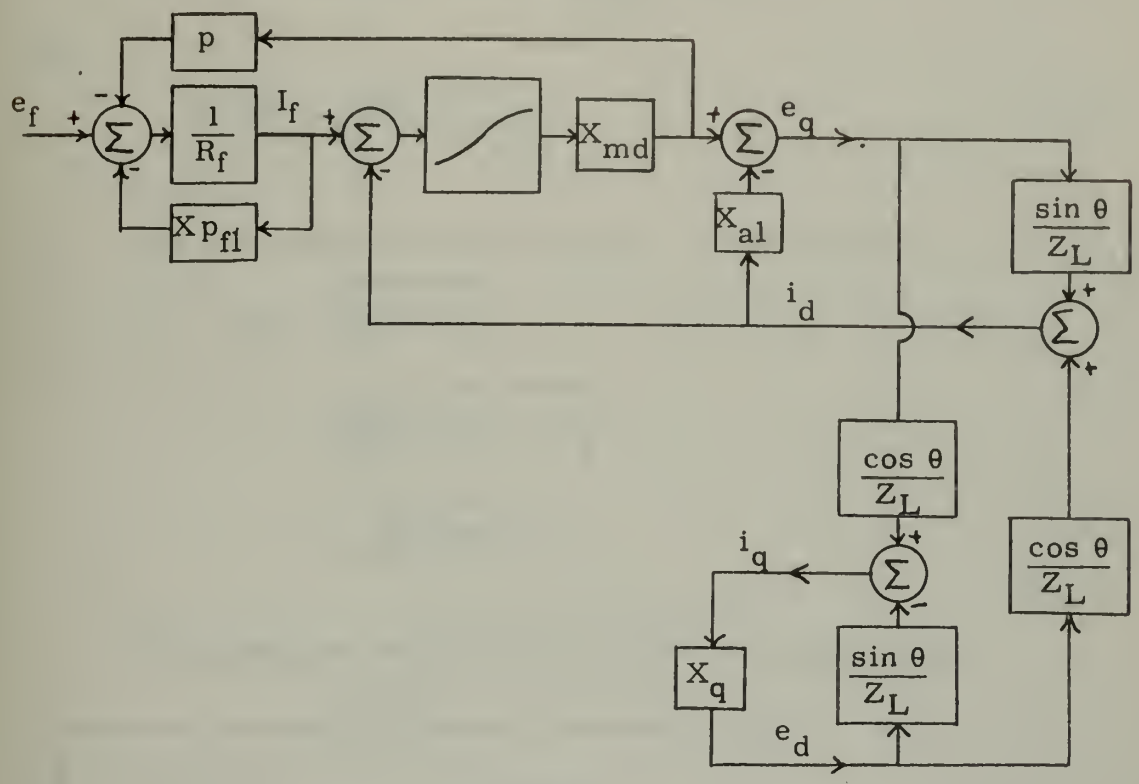

FIGURE (V)

The load portion of the block diagram can be further reduced if the load parameters are considered constant. For the experimental verification of the block diagram, Z_L and X_q are constant, and for a specific load condition, θ is constant. Thus, $e_d = f_1(e_q)$ and $i_d = f_2(e_q)$ for constant power factor.

Thus:

$$i_d = K_1(\theta)e_q \tag{13}$$

and

$$e_d = K_2(\theta)e_q \tag{14}$$

where:

$$K_1(\theta) = \frac{X_q \cos^2 \theta}{Z_L(Z_L + \sin \theta [X_q])} + \frac{\sin \theta}{Z_L} \tag{15}$$

and

$$K_2(\theta) = \frac{X_q \cos \theta}{Z_L + \sin \theta (X_q)} \tag{16}$$

The per phase terminal voltage e_t can be written

$$e_t = \sqrt{e_d^2 + e_q^2}$$

$$= \sqrt{[K_2(\theta) e_q]^2 + e_q^2}$$

$$= e_q \sqrt{[K_2(\theta)]^2 + 1} \tag{17}$$

Thus, the generator and load can be represented as

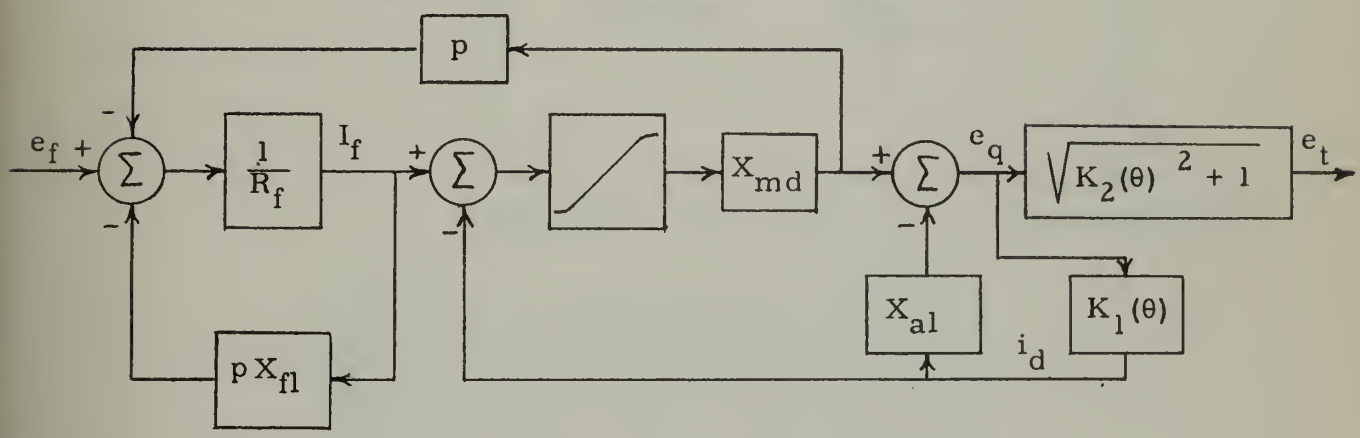

FIGURE (VI)

Computer Representation

The block diagram of figure (VI) is not directly solvable by analogue computer techniques because of the presence of differentiators. The representation of a differentiation on an analogue computer creates

an unusual amount of "noise" in the solution. It is therefore customary to transform a diagram involving differentiators into an equivalent diagram employing integrators only. The computer representation obtained is given in figure (VII). It should be noted that the saturation characteristic used is the inverse of that depicted in figure (VI).

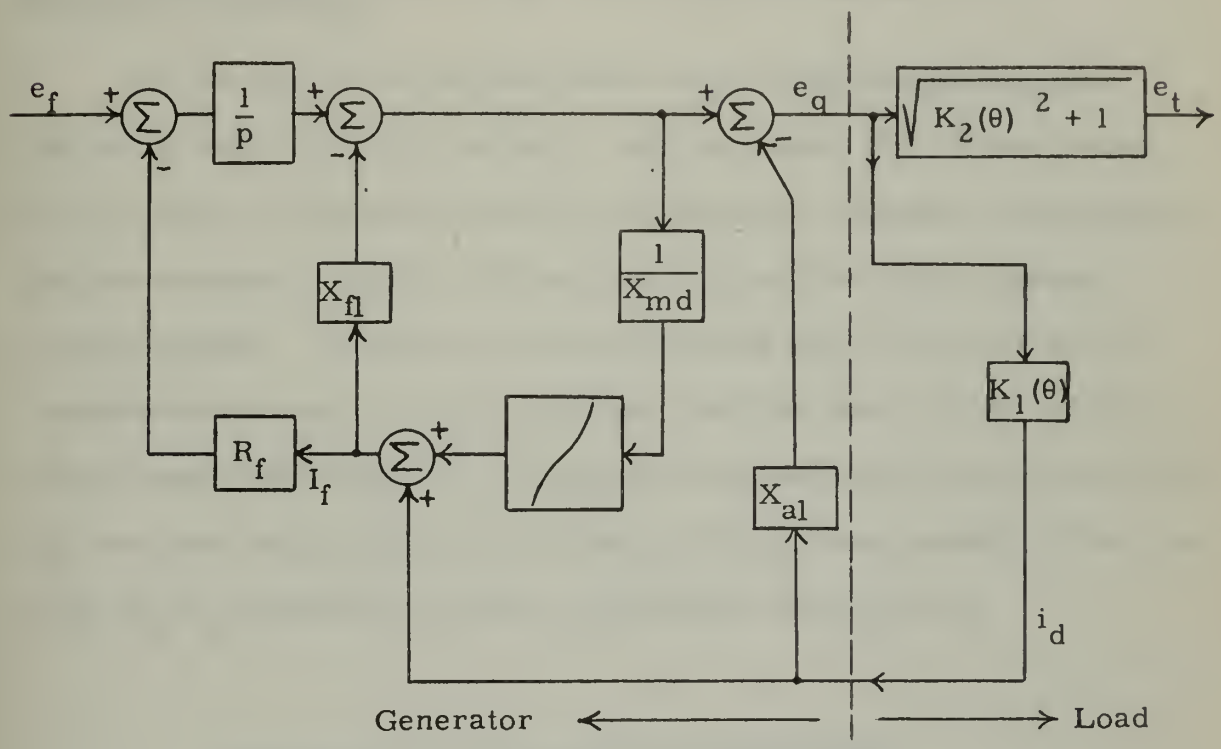

FIGURE (VII)

APPENDIX C

EXPERIMENTAL DETERMINATION OF MACHINE PARAMETERS AND TRANSIENT PHENOMENA

Machine Parameters

The various machine parameters were determined from the following tests and measurements: slip test, open circuit test, short circuit test, and a measurement of the field time constant. An oscillograph was used to record both the slip test and field time constant measurements. As shown by the calculations below, the direct axis synchronous reactance, X_d, was found from the short circuit and open circuit tests (see figure II). The quadrature axis synchronous reactance, X_q, was then calculated from the value of X_d already found and from the ratio X_q/X_d as determined from the slip test (see figure I).

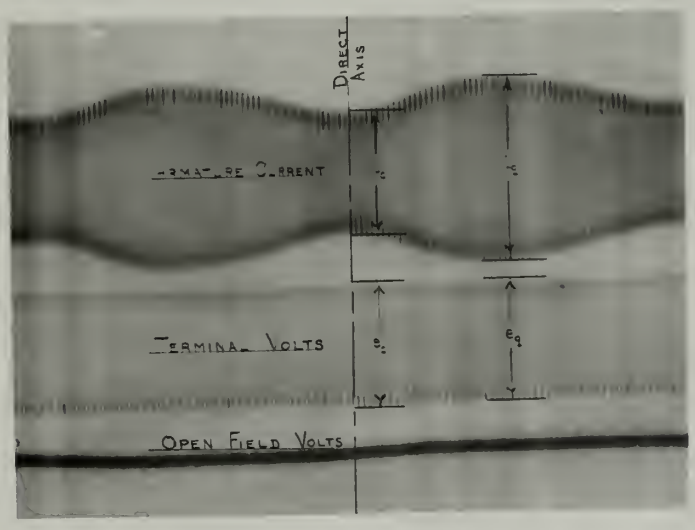

FIGURE I. SLIP TEST

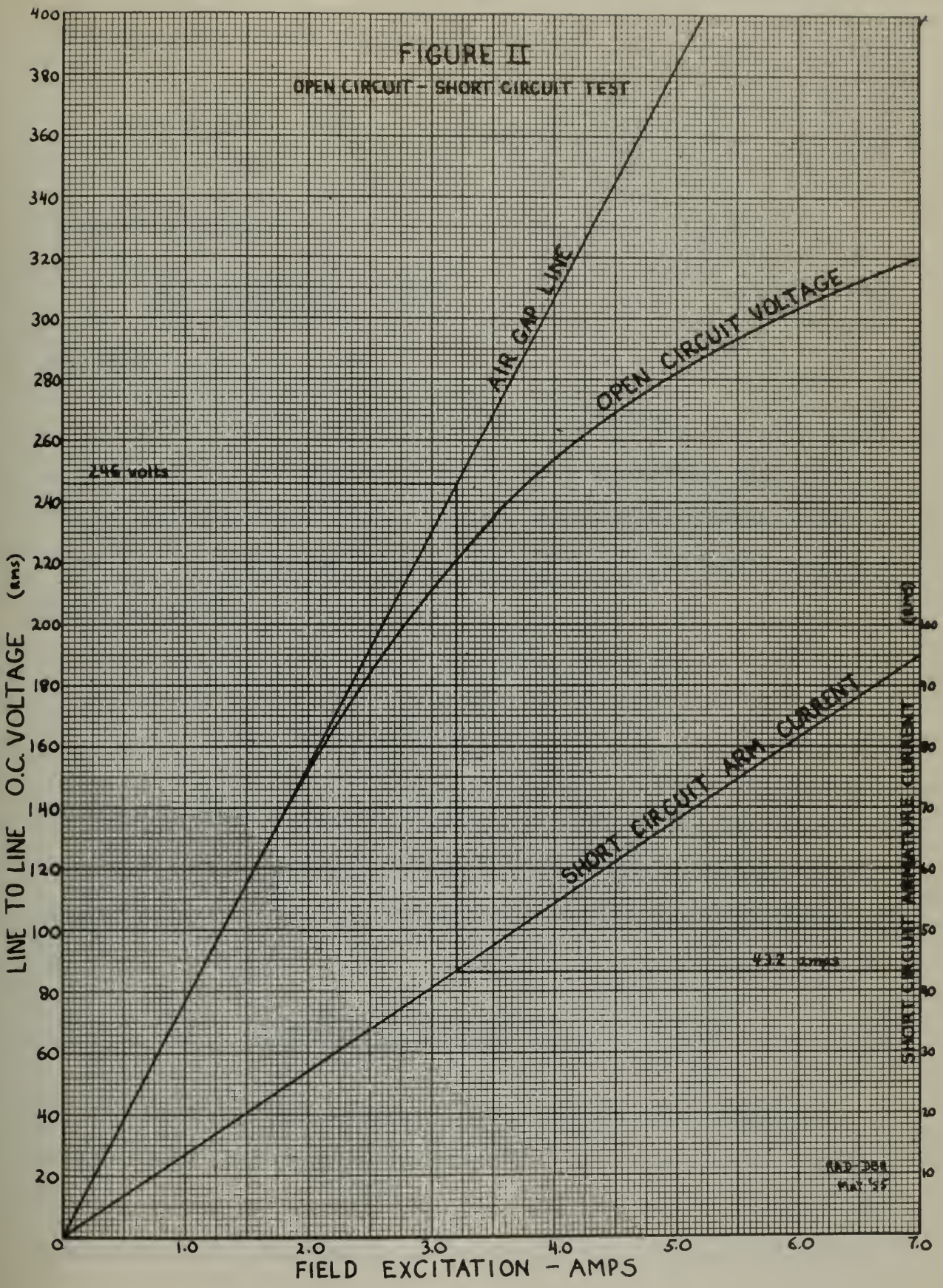
FIGURE II
OPEN CIRCUIT - SHORT CIRCUIT TEST
AIR GAP LINE
OPEN CIRCUIT VOLTAGE
SHORT CIRCUIT ARM. CURRENT
246 volts
432 amps
LINE TO LINE O.C. VOLTAGE (rms)
SHORT CIRCUIT ARMATURE CURRENT (amp)
FIELD EXCITATION - AMPS
0
1.0
2.0
3.0
4.0
5.0
6.0
7.0
20
40
60
80
100
120
140
160
180
200
220
240
260
280
300
320
340
360
380
400
10
20
30
40
50
60
70
80
90
100

From the short circuit and open circuit tests,

$$X_d = \frac{E_{f_{ag}}}{I_{a_{sc}}} = \frac{246}{43.2\sqrt{3}} = 3.285 \text{ ohms.} \tag{1}$$

From the slip test,

$$\frac{X_q}{X_d} = \frac{1.04/1.6}{1.06/1.08} = 0.662 \tag{2}$$

Therefore

$$X_q = 0.662\ X_d = (0.662)(3.285) = 2.175 \text{ ohms.} \tag{3}$$

The direct and quadrature synchronous reactances, X_d and X_q, can be expressed in per unit as the sum of an armature leakage reactance X_{al} and a reactance X_{ad} corresponding to the direct axis armature reaction flux:

$$X_d = X_{al} + X_{ad} \tag{4}$$

$$X_q = X_{al} + X_{aq} \tag{5}$$

In a similar manner the per unit field self reactance X_{ff} can also be expressed as the sum of a field leakage reactance X_{fl} and the field magnetizing reactance X_{fm}, which in the reciprocal per unit system (8) is equal to X_{md}.

$$X_{ff} = X_{fl} + X_{fm} = X_{fl} + X_{md} \tag{6}$$

In order to obtain an adequate block diagram representation it was necessary to determine the alternator field resistance R_f, a proper load representation, a method for insertions into the block diagram the nonlinear effects of saturation, and values for X_{fl}, X_{al}, and X_{md} which

have already been defined. For the computation of the values above, a reciprocal per unit system (8) was used in which base field current is so defined that X_{ad}, the reactance of direct axis armature reaction, is the equivalent per unit magnetizing reactance between armature and field, X_{md}. Therefore, base field current can be read directly on the air gap line of the no-load saturation curve corresponding to a per unit armature voltage equal to per unit X_{ad}.

Of the parameters needed for the block diagram, Appendix B describes the methods used to determine a load representation and the nonlinear saturation characteristic. The calculations below determine the remaining parameters: R_f, X_{fl}, X_{al}, and X_{md}. In all cases per unit values are found by the reciprocal system described in reference 8 and are referred to the armature.

The magnetizing reactance X_{md} and the armature leakage reactance X_{al} are found from the Potier triangle of figure (III). The distance ac is proportional to X_d, bc is proportional to $X_{ad} = X_{md}$, and ab is proportional to X_{al}. It follows that

$$\frac{X_{ad}}{X_d} = \frac{bc}{ac} = 0.7895 \tag{7}$$

and

$$\frac{X_{al}}{X_d} = \frac{ab}{ac} = 0.2105 \tag{8}$$

Using the value for X_d already determined,

$$X_{ad} = 0.7895\ X_d = 2.59 \quad \text{ohms} \tag{9}$$

$$X_{al} = 0.2105\ X_d = 0.692 \text{ ohms} \tag{10}$$

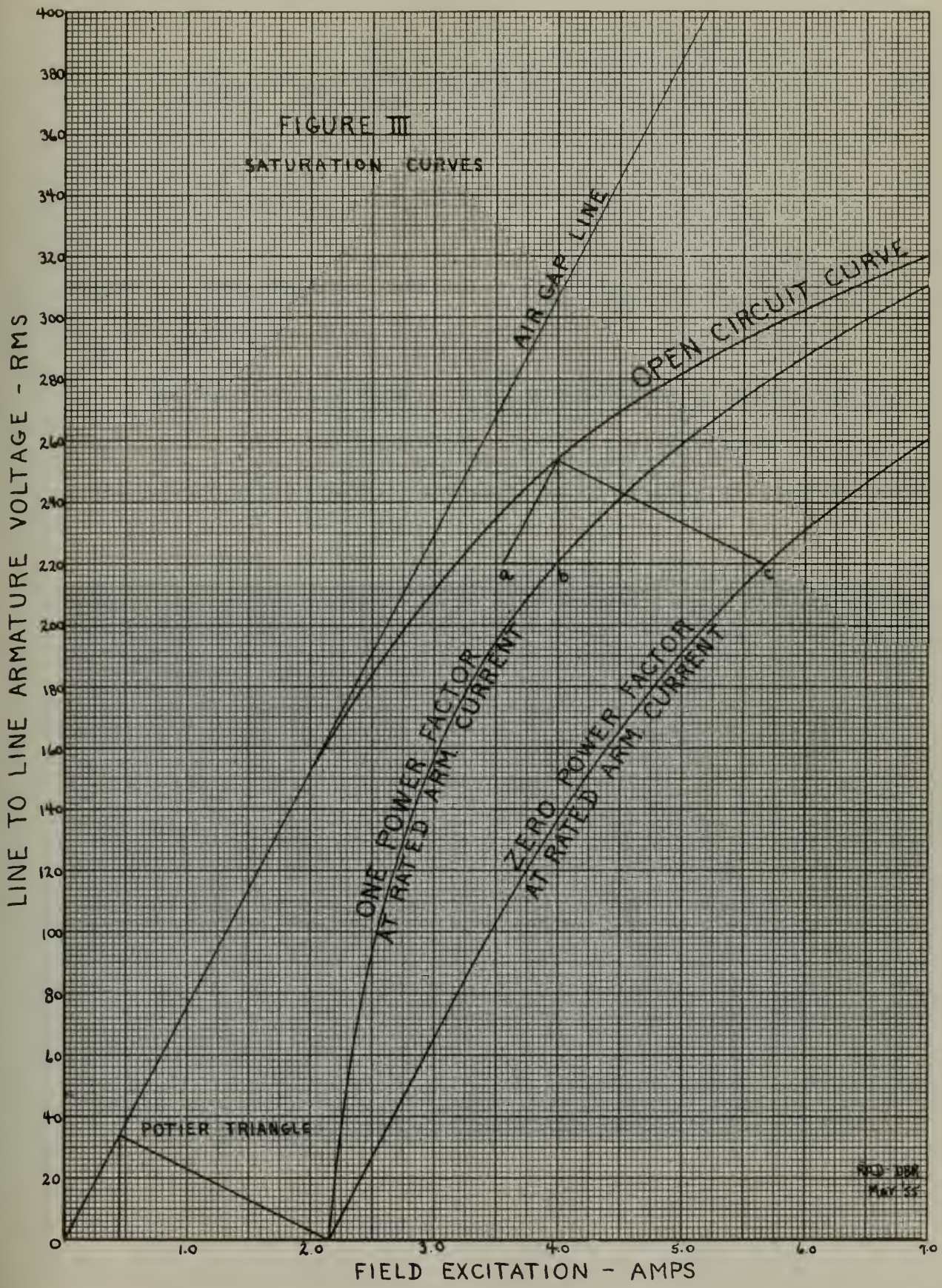
FIGURE III
SATURATION CURVES
AIR GAP LINE
OPEN CIRCUIT CURVE
ONE POWER FACTOR
AT RATED ARM. CURRENT
ZERO POWER FACTOR
AT RATED ARM. CURRENT
POTIER TRIANGLE
a
b
c
LINE TO LINE ARMATURE VOLTAGE - RMS
FIELD EXCITATION - AMPS
0
20
40
60
80
100
120
140
160
180
200
220
240
260
280
300
320
340
360
380
400
1.0
2.0
3.0
4.0
5.0
6.0
7.0
RED DBR
MAY '55

and in per unit values

$$X_{md} = X_{ad} = \frac{X_{ad}}{X_{ao}} = 0.592 \text{ per unit} \tag{11}$$

$$X_{al} = \frac{X_{al}}{X_{ao}} = 0.1576 \text{ per unit} \tag{12}$$

where the base armature reactance, $X_{ao} = e_{ao}/i_{ao} = 4.39$ ohms and e_{ao} and i_{ao} are nameplate values (peak).

The field leakage reactance X_{fl} was obtained by finding the field time constant from the application of a step change in field excitation and a record of the resulting transient on an oscillogram (see figure IV).

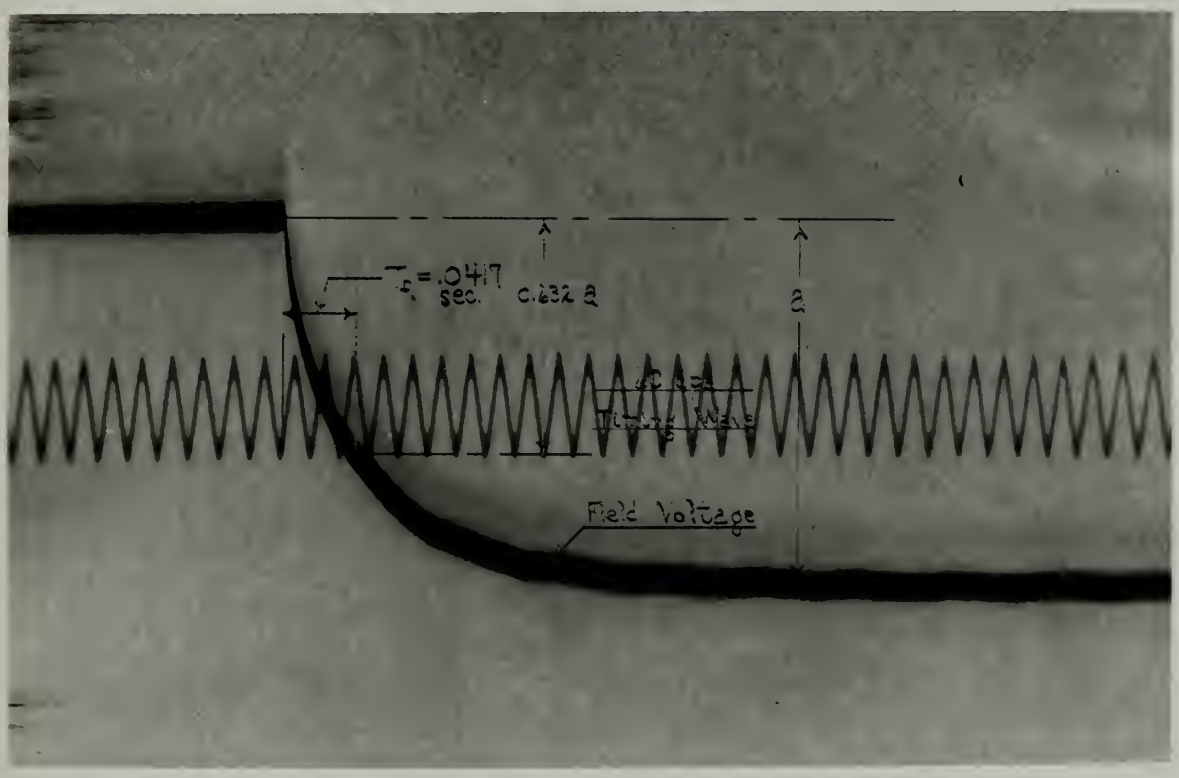

FIGURE (IV)

Thus, knowing the field time constant τ_f and having measured the field resistance R_f, the field inductance could be calculated.

$$L_f = \tau_f R_f = 6.96 \text{ henries} \tag{13}$$

The determination of per unit field self-reactance X_{ff} follows.

$$X_{ff} = \frac{3}{2} \frac{L_f}{L_{ao}} \left(\frac{i_{fo}}{3/2\, i_{ao}}\right)^2 = 0.69 \quad \text{per unit} \tag{14}$$

where $L_{ao} = X_{ao}/\omega$

i_{ao} = peak armature rated current

i_{fo} = base field current read on the air gap line of the no-load saturation curve corresponding to a per unit armature voltage equal to per unit X_{ad}.

= 1.7 amps

Since $X_{ff} = X_{fl} + X_{md}$,

$$x_{fl} = 0.69 - 0.592 = 0.098 \text{ per unit} \tag{15}$$

The only per unit values remaining to be found for a complete block diagram representation can be calculated from the following formulas:

$$X_{d_{(\text{per unit})}} = \frac{X_{d_{(\text{ohms})}}}{X_{ao}} = 0.749 \text{ per unit} \tag{16}$$

$$X_{q_{(\text{per unit})}} = \frac{X_{q_{(\text{ohms})}}}{X_{ao}} = 0.495 \text{ per unit} \tag{17}$$

$$R_{f_{(\text{per unit})}} = \frac{3}{2} \frac{R_{f_{(\text{ohms})}}}{X_{ao}} \left(\frac{i_{fo}}{3/2\, i_{ao}}\right)^2 = 2.63 \times 10^{-4}\ R_{f_{(\text{ohms})}} \tag{18}$$

$$e_{f_{(\text{per unit})}} = \frac{e_{f_{(\text{volts})}}}{e_{ao}} \left(\frac{i_{fo}}{3/2\, i_{ao}}\right) = 0.0173 \text{ per unit} \tag{19}$$

Transient Phenomena

The dynamic performance of the synchronous alternator was tested at three widely varying load conditions: pure inductive load (pF = 0), pure resistive load (pF = 1), and a combination inductive-resistive load (pF = 0.752). At each load condition step changes were applied to the alternator and the transient effects upon armature terminal voltage, armature current, and field voltage were recorded by means of oscillograms. The step changes consisted of going from full load to no load, going from no load to full load, and applying a step in the field excitation.

The oscillograms of figure (V) through (XIII) indicate the steady state values before and after each step change and the time constants associated with the transient phenomena for the three load conditions used.

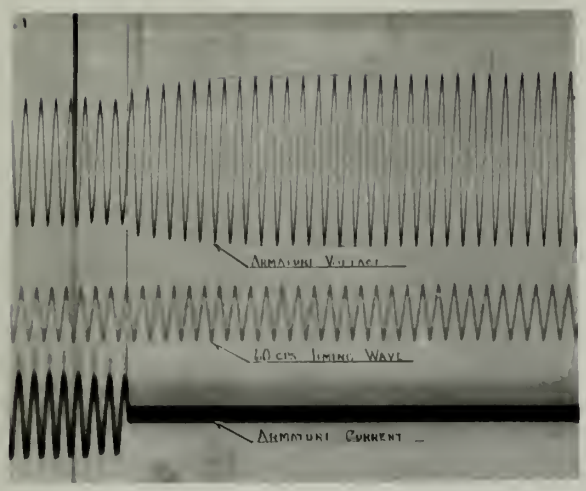

Figure V

Full Load to No Load

e_{t_1} = 0.988 per unit

e_{t_2} = 1.372 per unit

τ = 0.10 sec

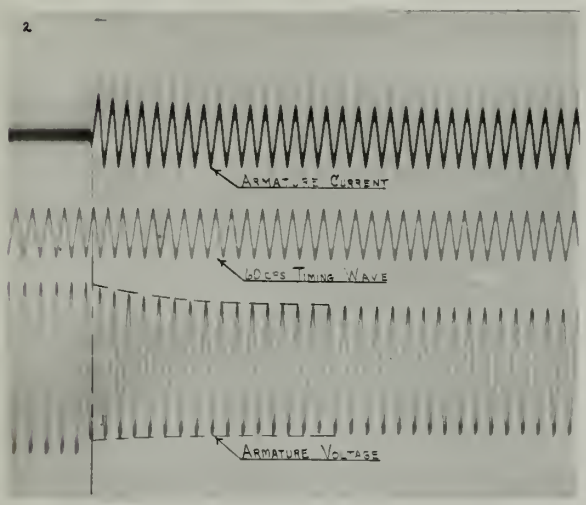

Figure VI

No Load to Full Load

e_{t_1} = 1.363 per unit

e_{t_2} = 0.982 per unit

τ = 0.125 sec.

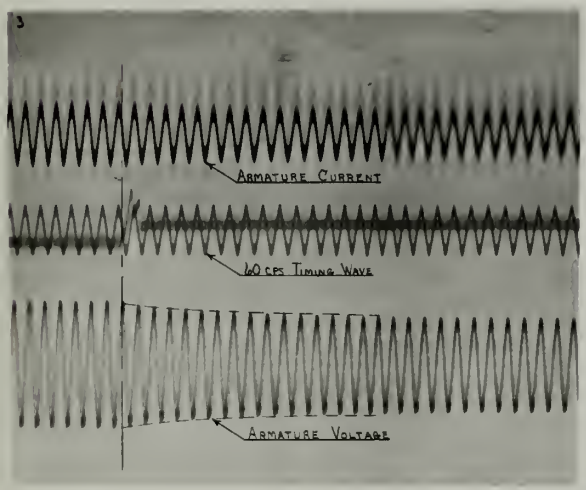

Figure VII

Field Step

e_{t_1} = 1.0 per unit

e_{t_2} = 0.705 per unit

τ = 0.155 sec.

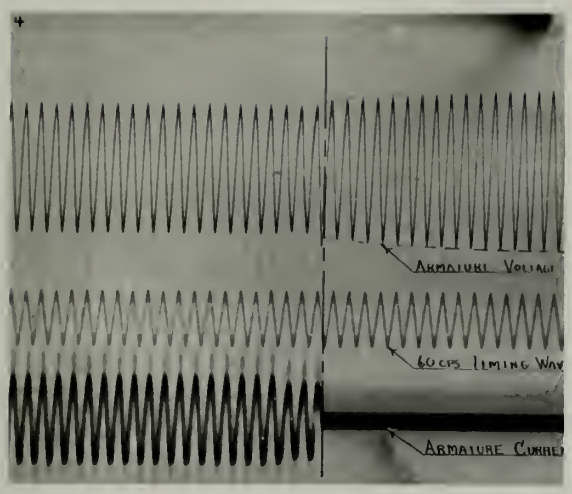

Figure VIII

Full Load to No Load

e_{t_1} = 1.0 per unit

e_{t_2} = 1.327 per unit

τ = 0.125 sec.

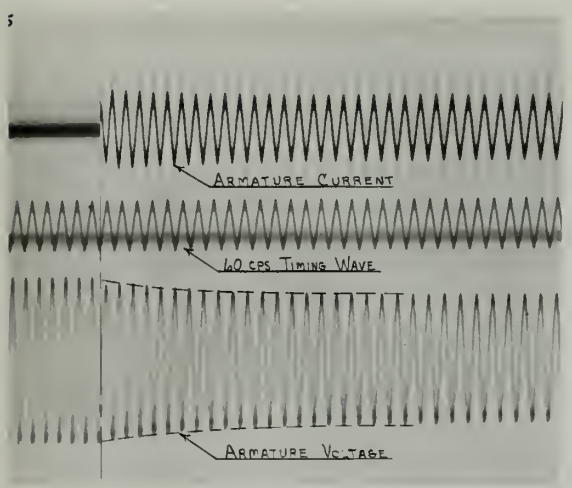

Figure IX

No Load to Full Load

e_{t_1} = 1.325 per unit

e_{t_2} = 0.988 per unit

τ = 0.130 sec.

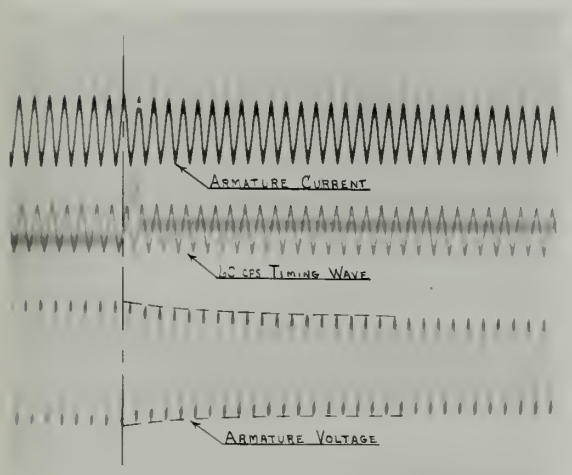

Figure X

Field Step

e_{t_1} = 1.0 per unit

e_{t_2} = 0.734 per unit

τ = 0.148 sec.

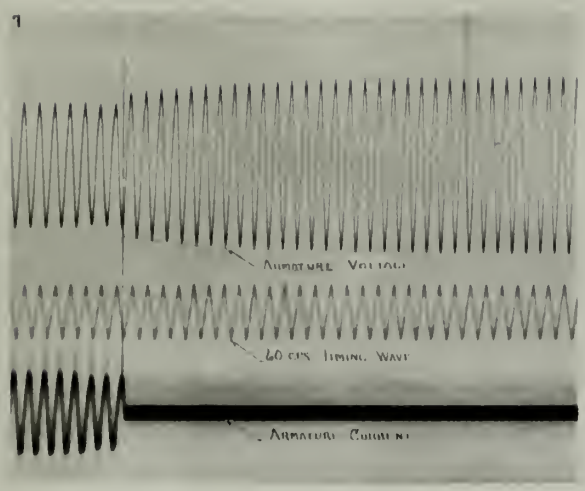

Figure XI

Full Load to No Load

e_{t_1} = 0.991 per unit

e_{t_2} = 1.446 per unit

τ = 0.11 sec.

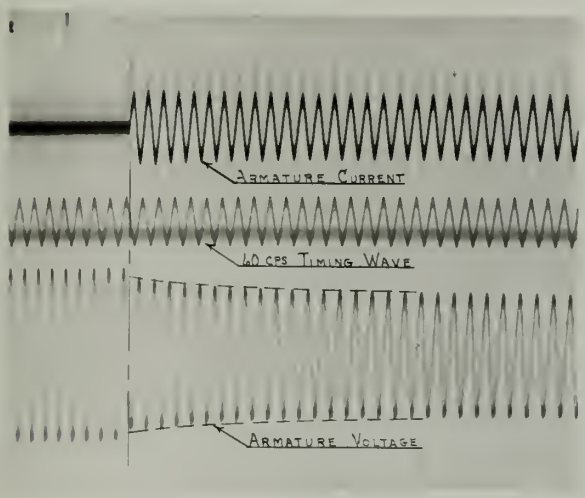

Figure XII

No Load to Full Load

e_{t_1} = 1.423 per unit

e_{t_2} = 0.978 per unit

τ = 0.14 sec.

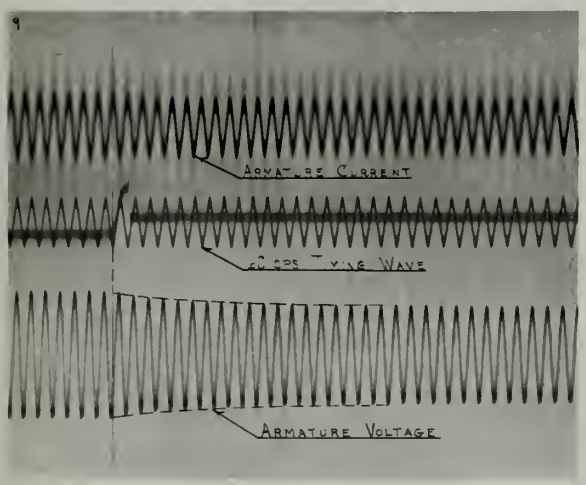

Figure XIII

Field Step

e_{t_1} = 1.009 per unit

e_{t_2} = 0.737 per unit

τ = 0.145 sec.

APPENDIX D

COMPUTER DETERMINATION OF TRANSIENT PHENOMENA

In order to check the validity of the synchronous generator representation developed in Appendix B, it is necessary to carry out both experimental and analytic tests which can be correlated in the transient and steady states. The purpose of this appendix is to obtain the analytic results of various changes in excitation and load conditions on the generator output.

One of the most difficult problems in the analysis and synthesis of the synchronous generator arises from consideration of saturation and other nonlinearities. The method employed in this thesis consists of concentrating all the generator nonlinearities at a single point in a block diagram which can be represented on an analog computer.

The principle of operation of the analog computer is based on the fact that analogies can be drawn among the various types of physical systems when the differential equations describing the systems are comparable. Of the various types of analog computers, the one most frequently used is the d-c analog computer in which direct voltages are used to represent the dependent variables. The simple computing networks in the d-c analog computer are made up of RLC networks and d-c amplifiers.

Although the analog computer can carry out the differentiation operation, the use of differentiators is avoided when possible because they tend to amplify signal noise and cause unwanted high frequency

oscillations. Usually when differentiators are present in a circuit they can be replaced with integrators by proper adjustment of the analog circuit.

There are several ways of representing system nonlinearities on the analog computer. The one resorted to in the solution of the synchronous generator problem is to construct a nonlinear characteristic curve relating the field current (I_{oc}) which causes an open circuit armature voltage, to a field current, (I_{ag}), which generates the same armature voltage on the air gap line of the open circuit characteristic curve. From the curve obtained, a photographic plate is prepared for use in the computer function generator. A signal input to the function generator causes a cathode ray beam to ride on the photographic contour generating a continuous output signal. Figure (I) shows the photographic plate used in the computer work described in this appendix.

FIGURE (I). COMPUTER FUNCTION GENERATOR PLATE

The block diagram of figure (VII), appendix B, must be represented on the analog computer in terms of the computer tools available; i.e., integrators, summers, potentiometers, voltages, etc. This representation is given in figure (II).

A shift in the time scale of the integrators was performed by dividing all integrator input potentiometer settings by the time scale, α_t. Thus, if α_t were 100, the computer time to perform a given operation would be one hundred times as long as for the real time alternator operation. This shift in time scale was made necessary for two reasons: to allow the transients to be recorded at a sufficiently slow speed that the dynamic response of the recording instruments would not be exceeded, and also to adjust the signal level of the integrator output to insure that the maximum signal level of 100 volts would not be exceeded.

The differential operator for this per unit work is taken equal to $d/d(\omega_o t)$ where ω_o is the electrical frequency of the generator, 120π radians per second. Thus, $p = (1/120\pi)p'$ where p' is d/dt. The integration term, $1/p$, therefore equals $(120\pi)(1/p')$. In order to reduce the per unit block diagram integration to a pure integration, the integrator output signal is then divided by 120π. The RC network shown at the input No. 8 summer is a stabilization network used to prevent system oscillation.

Transients are initiated by throwing a switch on the computer. The switch movements cause a step in the field voltage or a change in the load condition between full load and no load.

A preliminary step in the use of the computer is to check the steady-state values of field current vs. armature voltage for various

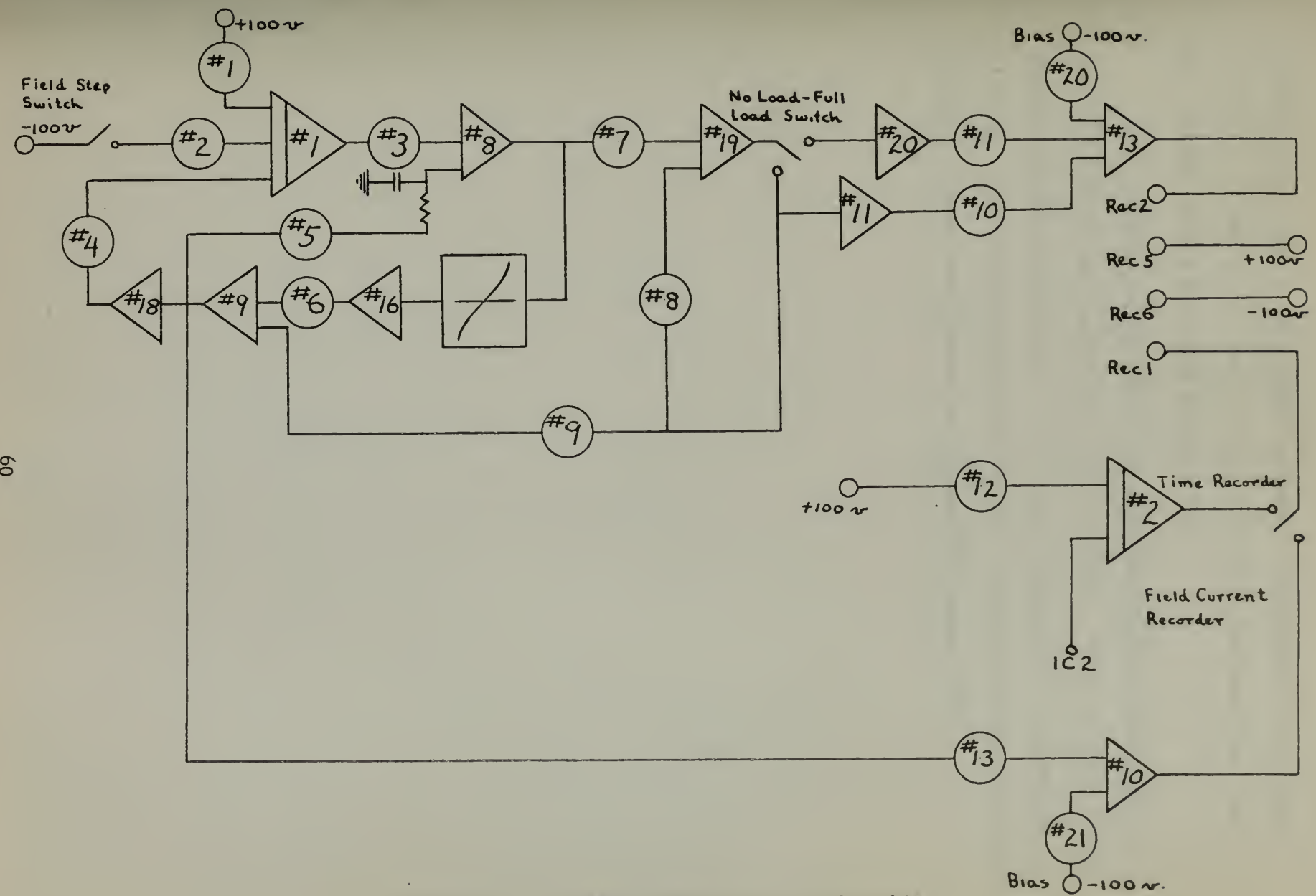

FIGURE II. COMPUTER CIRCUIT DIAGRAM

conditions of loading. This step consisted of obtaining the generator saturation curves for no load, 1.0 power factor, and zero power factor. These curves are given in figure (III).

The conditions under which the experimental work of appendix C was determined were duplicated on the computer. The computer potentiometer settings which were used for each solution are tabulated in table (I). The transient solutions obtained, with their steady-state and transient values, are pictured in figures (IV) through (XII).

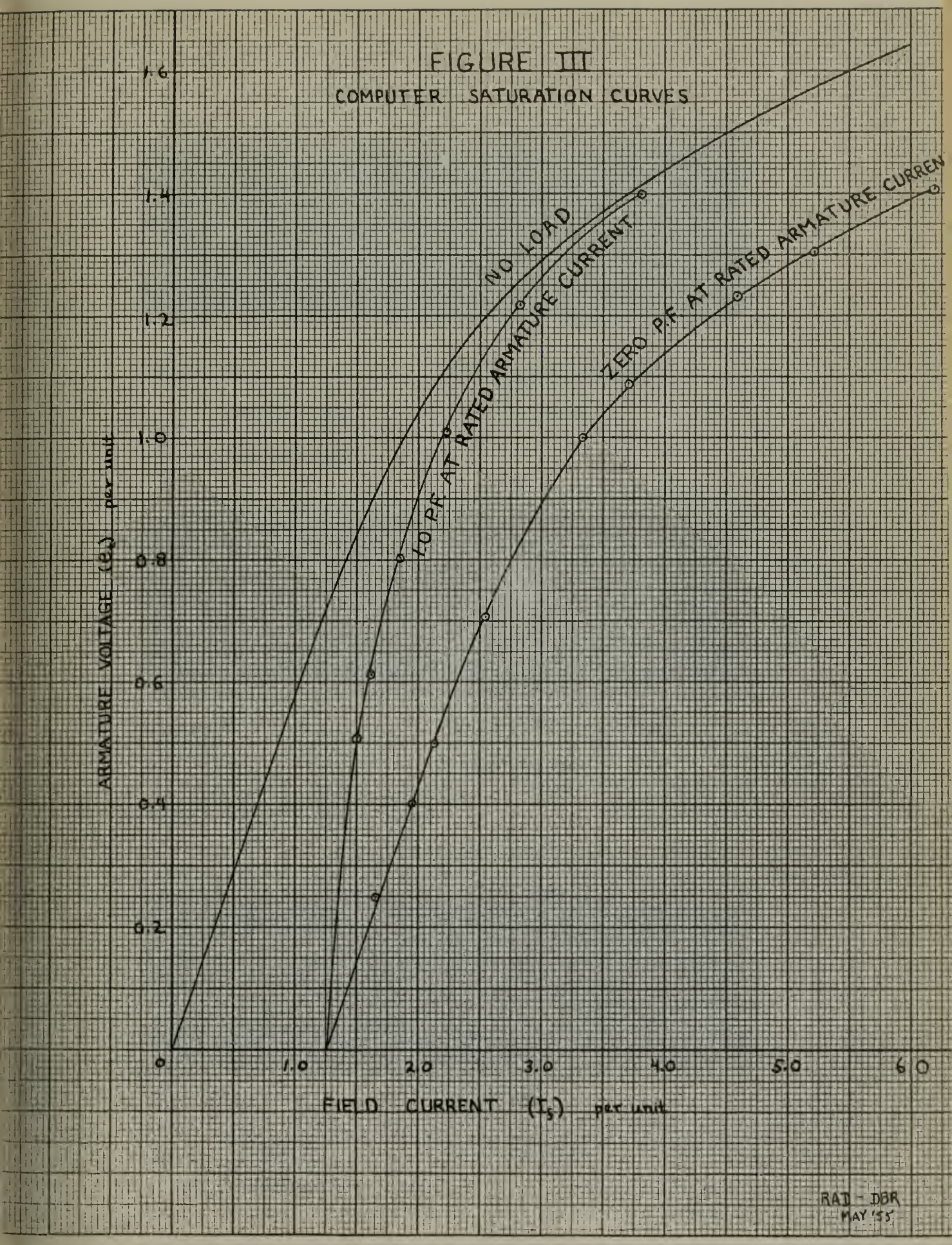
FIGURE III
COMPUTER SATURATION CURVES
NO LOAD
1.0 P.F. AT RATED ARMATURE CURRENT
ZERO P.F. AT RATED ARMATURE CURREN
ARMATURE VOLTAGE (E_a) per unit
FIELD CURRENT (I_f) per unit
0
0.2
0.4
0.6
0.8
1.0
1.2
1.4
1.6
1.0
2.0
3.0
4.0
5.0
6.0
RAD - DBR
MAY '55

Computer Transients - PF = 0

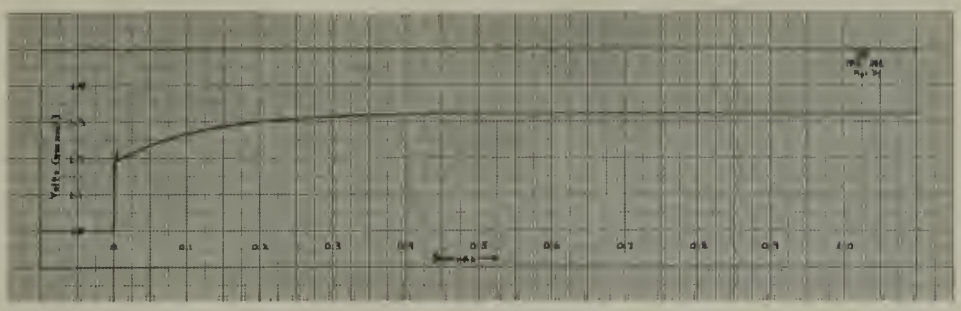

Figure IV — Full Load to No Load

e_{t_1} = 1.205 per unit — τ = 0.105 sec.

e_{t_2} = 1.332 per unit

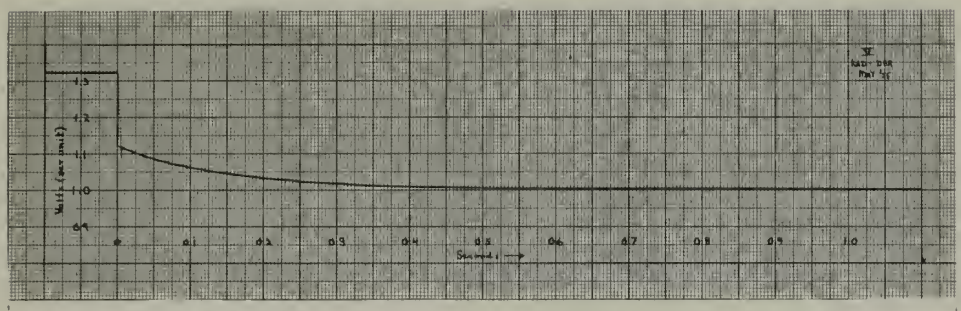

Figure V — No Load to Full Load

e_{t_1} = 1.108 per unit — τ = 0.145 sec.

e_{t_2} = 0.995 per unit

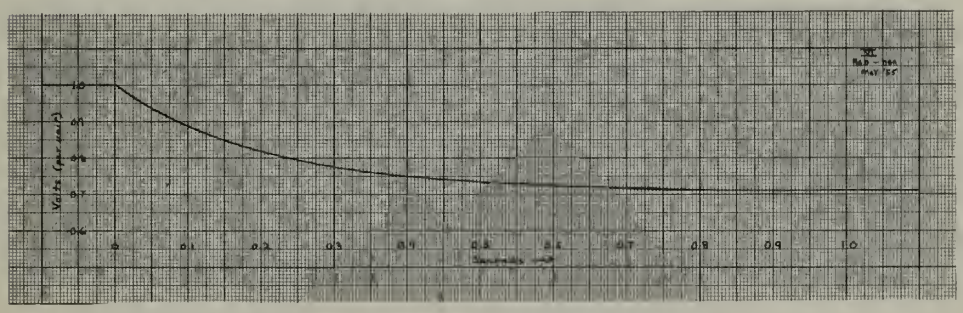

Figure VI — Field Step

e_{t_1} = 1.00 per unit — τ = 0.20 sec.

e_{t_2} = 0.66 per unit

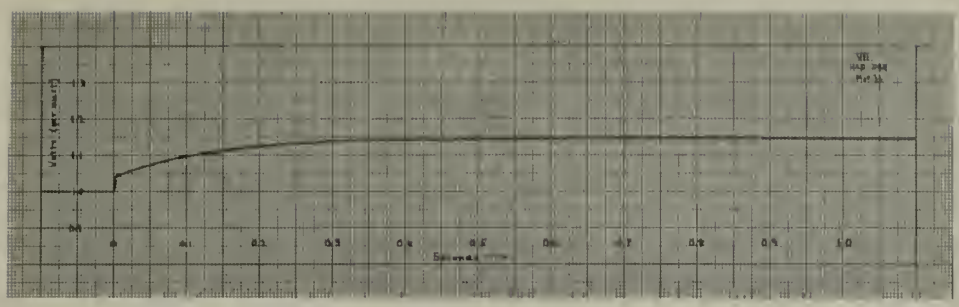

Figure VII Full Load to No Load

e_{t_1} = 1.0 per unit τ = 0.13 sec.

e_{t_2} = 1.11 per unit

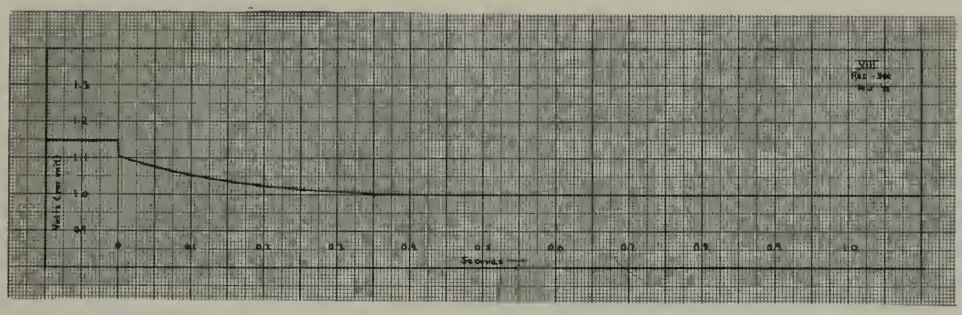

Figure VIII No Load to Full Load

e_{t_1} = 1.12 per unit τ = 0.14 sec.

e_{t_2} = 1.01 per unit

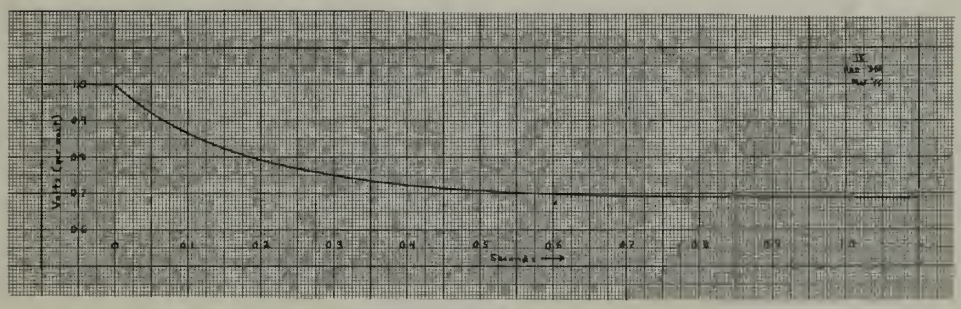

Figure IX Field Step

e_{t_1} = 1.00 per unit τ = 0.175 sec.

e_{t_2} = 0.62 per unit

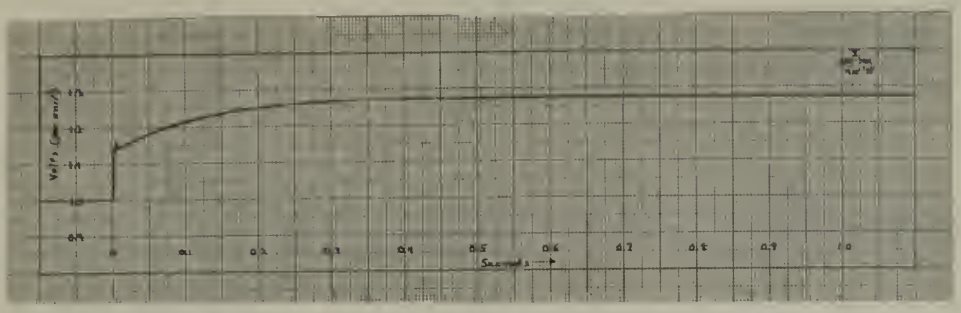

Figure X — Full Load to No Load

e_{t_1} = 1.142 per unit — τ = 0.10 sec

e_{t_2} = 1.28 per unit

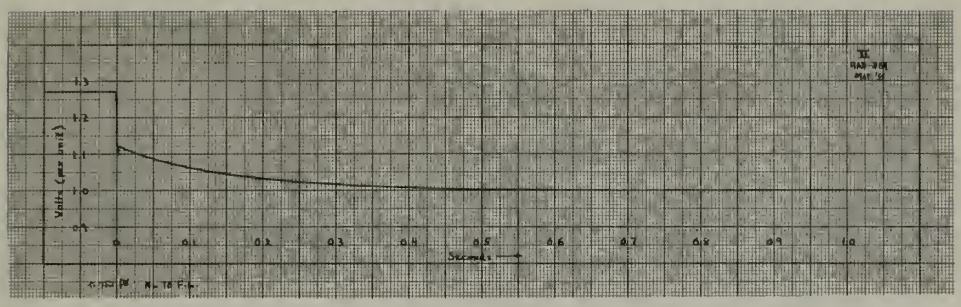

Figure XI — No Load to Full Load

e_{t_1} = 1.13 per unit — τ = 0.145 sec.

e_{t_2} = 1.0 per unit

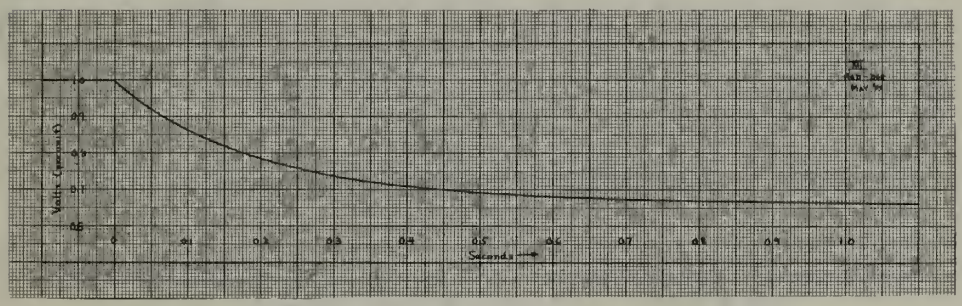

Figure XII — Field Step

e_{t_1} = 1.00 per unit — τ = 0.195 sec.

e_{t_2} = 0.60 per unit

TABLE I

STEADY STATE POTENTIOMETER SETTINGS

Potentiometers	(1) $\frac{160\, e_f}{a_t}$	(2) $\frac{160\, \Delta e_f}{a_t}$	(3) $\frac{0.801}{X_{md}}$ x 1/4	(4) $\frac{1067\, R_f}{a_t}$	(5) $\frac{2.27\, X_{fl}}{X_{md}}$	(6) 0.8825	(7) $0.4415\, X_{md}$	(8) $k_1 X_{al}$
No Load Saturation Curve	0.0277		0.3476	Varied	0.3777	0.8852	0.2623	
Zero pF Saturation Curve (i_a = 1.0 p.u.)	0.0277		0.3476		0.3777	0.8852	0.2623	0.1579 Will vary in proportion shown for various points on curve
One pF Saturation Curve (i_a = 1.0 p.u.) Z_L = 0.5	0.0277		0.3476		0.3777	0.8852	0.2623	0.314
0.6								0.2175
0.8								0.1222
1.0								0.078
1.2								0.0541
1.4								0.0398

STEADY STATE POTENTIOMETER SETTINGS (CONT' D)

Potentiometers	(9) k_1	(10) $6.67\sqrt{k_2^2+1}$	(11) 6.67	(12) $\frac{1.333}{a_t}$	(13) 0.889
	x 1/4	x 1/10	x 1/10		
No Load Saturation Curve			0.708		0.8916
Zero pF Saturation Curve (i_a = 1.0 p.u.)	0.2555 will vary in proportion shown for various points on curve	0.708			0.8916
One pF Saturation Curve (i_a = 1.0 p.u.)					
Z_L = 0.5	0.5099	0.952			0.8916
0.6	0.3532	0.8888			↓
0.8	0.1972	0.8181			↓
1.0	0.1255	0.7817			↓
1.2	0.0866	0.7609			↓
1.4	0.0635	0.7470			↓

TABLE I (CONT'D)

TRANSIENT POTENTIOMETER SETTINGS

Potentiometers	(1)	(2)	(3)	(4)	(5)	(6)	(7)	(8)
pF = 0								
(1) F.L. to N.L.	0.0277		0.3476	0.0576	0.3777	0.8852	0.2623	0.1579
(2) N.L. to F.L.	↓		↓	↓	↓	↓	↓	↓
(3) Field Step	↓	0.0104	↓	↓	↓	↓	↓	↓
pF = 1								
(4) F.L. to N.L.	0.0277		0.3476	0.079	0.3777	0.8852	0.2623	0.078
(5) N.L. to F.L.	↓		↓	↓	↓	↓	↓	↓
(6) Field Step	↓	0.0106	↓	↓	↓	↓	↓	↓
pF = 0.752								
(7) F.L. to N.L.	0.0277		0.3476	0.0637	0.3777	0.8852	0.2623	0.1375
(8) N.L. to F.L.	↓		↓	↓	↓	↓	↓	↓
(9) Field Step	↓	0.0114	↓	↓	↓	↓	↓	↓

TRANSIENT POTENTIOMETER SETTINGS (CONT' D)

Potentiometers	(9)	(10)	(11)	(12)	(13)
pF = 0					
(1) F. L. to N. L.	0.2555	0.708	0.708	0.0133	
(2) N. L. to F. L.	↓	↓	↓	↓	
(3) Field Step					
pF = 1					
(4) F. L. to N. L.	0.1255	0.7817	0.708	0.0133	
(5) N. L. to F. L.	↓	↓	↓	↓	
(6) Field Step					
pF = 0.752					
(7) F. L. to N. L.	0.2218	0.733	0.708	0.0133	
(8) N. L. to F. L.	↓	↓	↓	↓	
(9) Field Step					

APPENDIX E

SUMMARY OF DATA AND CALCULATIONS

Definition of Parameters

e_f = field voltage

e_d = direct axis armature voltage

e_q = quadrature axis armature voltage

e_{ao} = peak armature rated voltage, line to line

e_t = $\sqrt{e_d^2 + e_q^2}$ = armature terminal voltage

i_f = field current

i_d = direct axis armature current

i_q = quadrature axis armature current

i_{ao} = peak armature rated current, per phase

i_t = $\sqrt{i_d^2 + i_q^2}$ = armature terminal current, per phase

X_{ff} = field self reactance

X_{fm} = field magnetizing reactance

X_{fl} = field leakage reactance

X_d = direct axis synchronous reactance

X_q = quadrature axis synchronous reactance

X_{ao} = e_{ao}/I_{ao} = base armature reactance

X_{al} = armature leakage reactance

X_{ad} = reactance of the direct axis armature reaction

X_{aq} = reactance of the quadrature axis armature reaction

X_{md} = magnetizing reactance between armature and field

M = mutual inductance between armature and field

L_d = direct axis synchronous inductance

L_q = quadrature axis synchronous inductance

R_f = field resistance

τ_f = open circuit field time constant

Z_L = load impedance

ω_o = rated electrical frequency

Summary

Parameter	Actual values	Per unit values
e_{ao}	$220\sqrt{2}$ volts	
i_{ao}	$28.9\sqrt{2}$ amps	
X_{ao}	4.39 ohms	
L_{ao}	0.01164 henries	
ω_o	120π rad/sec	1.0
e_f	112 volts	0.0173
X_d	3.285 ohms	0.749
X_q	2.175 ohms	0.495
X_{ad}	2.59 ohms	0.592
X_{md}		0.592
X_{al}	0.692 ohms	0.1576
X_{ff}		0.69
X_{fl}		0.098
τ_f	0.0417 sec	

APPENDIX F

EQUIPMENT

Generator

Westinghouse synchronous alternator, salient pole (rotor), with amortisseur windings.

KVA	11	% pF	90
Volts	220	Excitation Volts	125
Amps	28.9	Excitation Amps	5
Cycles	60	Style No.	897363
RPM	1200	Serial No.	1/5c3982

Driving Motor

Westinghouse direct current motor, shunt wound.

Volts	230	Serial No.	955771
Open Intermittent H. P.	15	Type	RF 10
Speed	550/1650	Form	A17

Computer

Reeves Electronic Analog Computer (REAC).

APPENDIX G

LITERATURE CITATIONS

1. H. C. Anderson, Jr., Voltage Variation of Suddenly Loaded Generators, G. E. Review, August, 1945.

2. C. Concordia, Synchronous Machines, J. Wiley and Sons, New York, 1951.

3. S. B. Crary, Power System Stability, Vol. I and II, J. Wiley and Sons, New York, 1945 and 1947.

4. A. E. Fitzgerald and C. Kingsley, Jr., Electric Machinery, McGraw-Hill Book Co., Inc., New York, 1952.

5. V. C. Halloway, Transient Characteristics of Aircraft Alternating Current Generators, AIEE Trans., Paper 54-305, 1954.

6. H. B. James, The Use of an Analogue Computer to Optimize the Transient Response of an Aircraft-Type Generator Regulator System, AIEE Tech. Paper 53-368, 1953.

7. L. A. Kilgore, Calculation of Synchronous Machine Constants, AIEE Trans., Vol. 50, pg. 1201, 1931.

8. A. W. Rankin, Per Unit Impedances of Synchronous Machines, AIEE Trans., Vol. 64, Part I, pp. 569-573, Part II, pp. 839-841, 1945.

9. C. F. Wagner, Machine Characteristics, Westinghouse Electrical Transmission and Distribution Reference Book, 1950

10. MIT Course 6.06 Notes, Electric Power Modulators, MIT Electrical Engineering Department Staff, 1954.

11. Wright Air Development Center Interim Engineering Report No. 2, General Specifications for Generator and Regulator Alternating Current, 1953.

12. Wright Air Development Center Technical Report 54-298, Study of Voltage Regulating Systems for Aircraft Alternating Current Generators, Part I, 1954.

13. REAC Analog Computer Theory and Operation Manual, EE Staff, MIT, 1954.

14 III 77 24037

Thesis
D787 28933

Duin
A dynamic representation of a salient pole synchronous generator.

14 III 77 24037

Thesis
D787 28933

Duin
A dynamic representation of a salient pole synchronous generator.

thesD787
A dynamic representation of a salient po
3 2768 001 89543 6
DUDLEY KNOX LIBRARY